Volume: 32 (2), Dec 2024 ISSN: 0970 - 1842

JAS Journal of Anatomical Sciences

(U.P. Chapter of Anatomical Society of India)

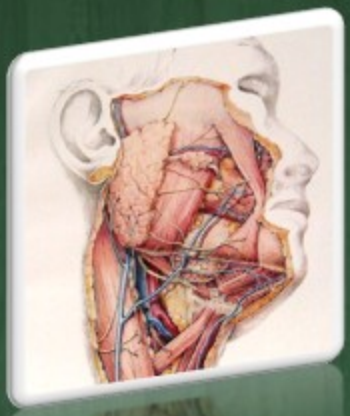
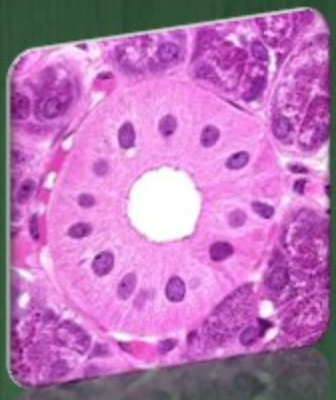

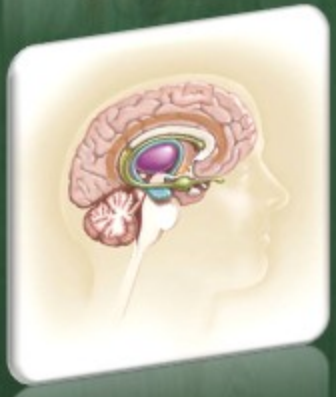

Editor-in-Chief
Dr. Satyam Khare

Joint Editor
Dr. Shilpi Jain


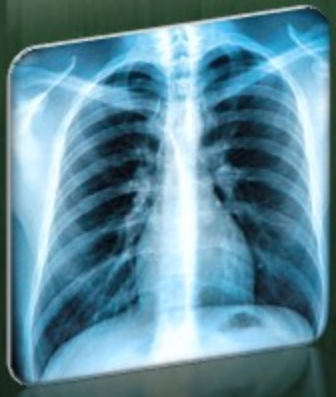

www.asiupjas.com

https://doi.org/10.46351/jas.v32i2pp53-65

JAS Journal of Anatomical Sciences (U.P. Chapter of Anatomical Society of India)

Original Article

Pedographic and radiographic analysis of foot and its clinical implication

Puneet Chaudhary[1], Swati Saxena[1], Rajesh Kumar Maurya[1], Mahendra Kumar Pant[1]

1. Department of Anatomy, Government Doon Medical College, Dehradun, India

ABSTRACT

Introduction: Foot posture plays a crucial role in musculoskeletal health by influencing the dynamic function and alignment of the lower limbs. Alterations in foot biomechanics, such as flatfoot, have been linked to the development and progression of medial compartment knee osteoarthritis (OA). Pedography, a non-invasive technique to assess foot posture, provides detailed visualization of footprints and may serve as an effective screening tool for early identification and management of foot malalignment using orthotics.

Materials and Methods: This case-control study assessed pedographic parameters (Arch index and Arch angle) and radiographic parameters (calcaneal pitch angle and cuboid abduction angle) in 45 patients with clinically and radiologically confirmed medial knee OA and 33 age-matched healthy controls from the Dehradun district. Additional radiographic angles measured included Meary's angle, talo-calcaneal angle, and talo-navicular coverage angle. The correlation between pedographic and radiographic parameters was analyzed, along with demographic factors such as BMI, age, and gender.

Results: Significant differences were found in both pedographic and radiographic measurements between individuals with and without knee OA. Pronated foot posture (elevated Arch index and reduced Arch angle) was more prevalent in the OA group. The cuboid abduction angle (CAA) and calcaneal pitch angle (CPA) also showed significant associations with OA status ($p = 0.000$ and 0.035, respectively). BMI was significantly associated with OA presence.

Conclusions: Pronated flatfoot was more common in individuals with medial knee OA, suggesting a biomechanical link. Pedographic assessment offers a useful, radiation-free alternative for early screening and prevention strategies, especially in rural settings where radiographic resources are limited.

Keywords: Arch index, Calcaneal pitch, Foot health, BMI, Foot alignment

Address for Correspondence:
Dr. Swati Saxena, Assistant Professor, Department of Anatomy, Government Doon Medical College, Dehradun, India
Email: 21swatidocsaxena@gmail.com

Date of Receiving: 19 Aug 2024
Date of Acceptance: 23 Sep 2024

INTRODUCTION

Osteoarthritis (OA) of the knee is a painful joint condition that damages the articular cartilage and bone structure. There has been evidence linking the symptoms of osteoarthritis (OA) to abnormal mechanical stress of the lower limbs [1,2]. The foot serves as essential for maintaining proper joint motion, absorbing ground reaction stresses, and creating the pattern of postural alignment within the lower extremities [3]. While doing weight-bearing tasks, the foot and knee move in a closed kinematic chain, which can cause excessive knee rotation in those who have flat feet [4]. thereby increasing the prevalence of OA [5,6]. It has been proposed that the conservative treatment of lower limb OA may benefit from orthoses that modify the features of the hindfoot.

For OA of the knee's medial compartment, lateral wedged insoles have been suggested. Given that the leading cause of pain and impairment in the elderly is osteoarthritis (OA) of the knee [6-11]. The aim of this study was to analyse the pedographic (arch angle and the arch index) and radiographic parameters (calcaneal pitch angle and cuboid abduction angle) of foot with and without medial knee osteoarthritis among the population in Dehradun district. The objectives of this study were:

1. To assess the correlation between the pedography parameters (arch index and arch angle) and socio-demographic factors such as age, gender, and BMI.
2. To estimate the frequency of MKOA related to age, gender and BMI.
3. To examine the correlation between the pedography parameters (arch index and arch angle) of foot and radiographic measurements in clinically diagnosed medial knee osteoarthritis.

MATERIAL AND METHODS

The present study was designed as a case control study and was carried out in Orthopaedics, Physical medicine and rehabilitation and Radiology departments of Government Doon hospital. Ethical clearance was obtained from Institutional Ethics Committee (IEC), GDMC, Dehradun via reference number: GDMC/ IEC/ 2023/ 28. This study included, 45 subjects (30 females and 15 males) with clinically diagnose medial knee osteoarthritis and 33 people without knee osteoarthritis (20 males and 13 females) to assess pedographic parameters, radiographic parameters and demographic parameters.

Samples were taken from patients who visited in departments of orthopaedics and PMR of government doon Hospital, Dehradun. Footprint were taken from Harris mat and x-ray foot were collected from department of radiology in Government Doon hospital, Dehradun.

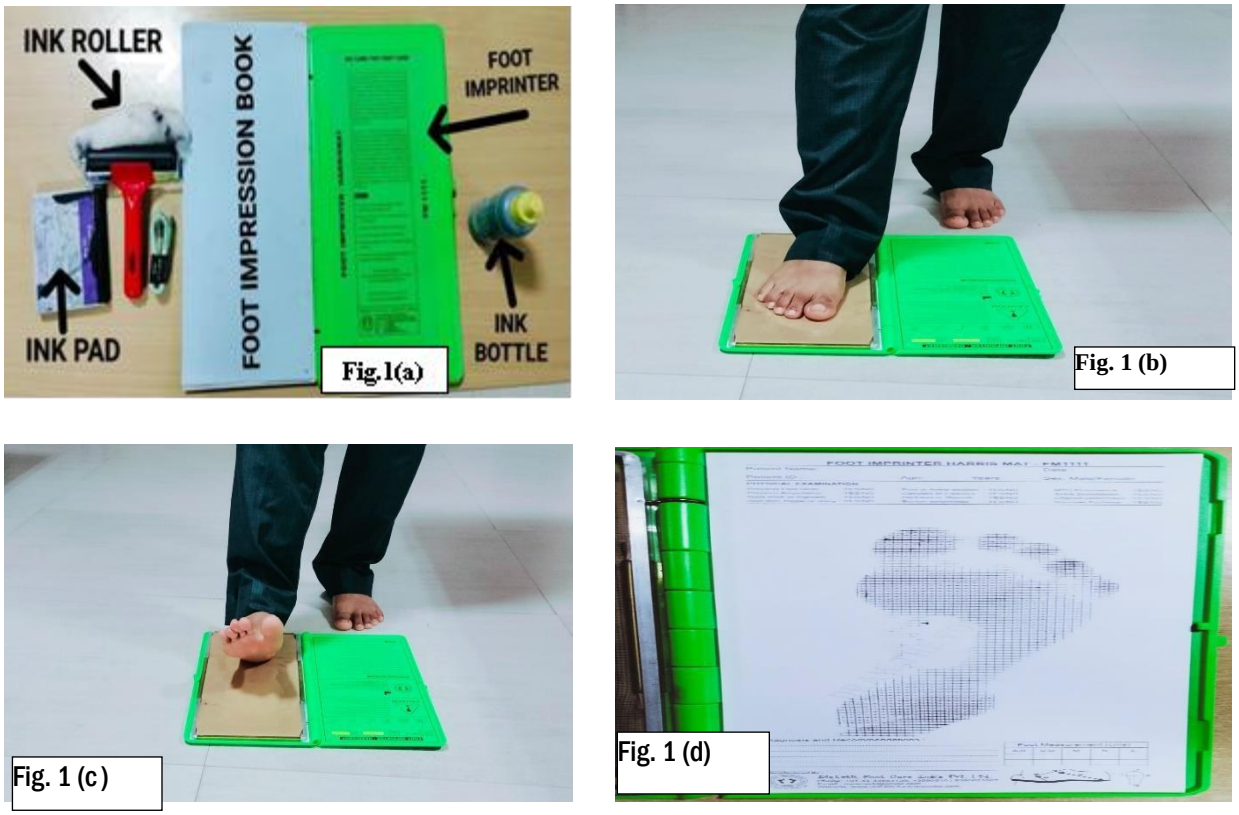

Fig. 1. Estimation of patients' footprint using Harris mat.

Inclusion criteria – Patients with previously or freshly diagnosed knee osteoarthritis, without having previous history of foot or ankle injury or walking deformity/gait with age 30-70 years.

Exclusion criteria - Patients with previous injury of foot or ankle, age <30 and >70 years, previous ankle or foot surgery, with foot prosthesis or orthosis, congenital deformity of foot and patients suffering from neurological disease eg -: hypotonia, cerebral palsy with muscular disease eg-: muscular dystrophy.

Procedure

Samples of cases were collected from patients who visited the PMR and Orthopaedics out patient departments. Participants' body mass index (BMI), height and footprint from Harris mat (Fig.1) were recorded.

Foot posture measurements:

Arch index: Using computer graphics, it was computed as the ratio of the middle portion to the total footprint area (Fig. 2(a)). A flatter (more pronated) foot was indicated by higher arch index values. flat foot= >0.26, normal=0.21-0.26, high arched=<0.26 [12].

Arch angle/Clarke's angle: It was measured as the angle formed by the line joining the metatarsal region's most medial point and the footprint's medial boundary line Fig. 2(b) [12].

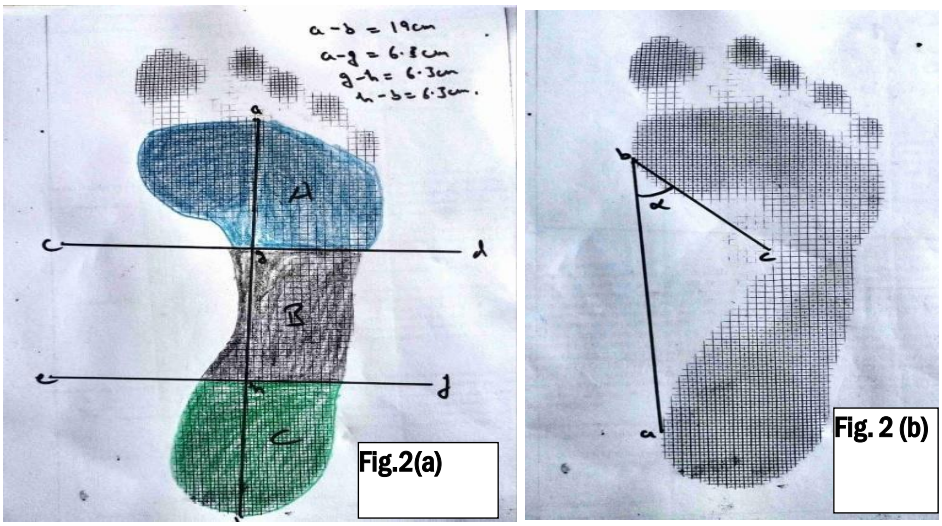

Fig. 2. Measurement of (a) Arch index and (b) Arch angle/Clarke's angle.

Radiographic Measurements:-

Calcaneal pitch angle: A line drawn on the plantar surface from the calcaneus and a segment joining the inferior border of the calcaneus and the inferior margin of the fifth metatarsal head constituted the calcaneal pitch angle (β). Fig. 3(a) [13].

Meary's angle(α): Created by the talus's long axis and the first metatarsal axis Fig. 3(b) [13].

Talo-navicular angle: The line that connects the medial and lateral edges of the talus and the line that connects the medial and lateral borders of the navicular bone are perpendicular enough to create (Y). Fig. 3(c) [13].

Cuboid abduction angle (CAA): Angle between the rearfoot's longitudinal axis and a line perpendicular to the cuboid's lateral surface (Fig. 2) (normal: 0°-5°). With the mid-tarsal joint pronating, this angle rises above 5°, and with supination and adduction, it falls below 0°. Fig. 3(d) [14].

Statical analysis: A Microsoft Excel sheet was used to tabulate and statistically analyze the data. The mean and standard deviation were used to express the findings with their p-value and correlation was calculated with the help of Pearson's coefficient.

RESULTS

A total of 78 participants were included in the study, with 45 individuals clinically diagnosed with medial knee osteoarthritis (MKOA) and 33 controls without MKOA. The mean age was higher in the OA group, and a greater proportion of females (30 out of 45) were affected compared to males (15 out of 45). Body Mass Index (BMI) was significantly higher in participants with MKOA (30.47±4.02) than in controls (22.96±2.7), with a highly significant p-value of 0.000.

Pedographic measurements revealed a significantly elevated arch index in the MKOA group (0.2813±0.045) compared to controls (0.2427±.023), indicating a flatter foot profile in OA participants (p = 0.000). Correspondingly, the arch angle (Clarke's angle) was significantly lower in the OA group (30.94±7.85°) than in controls (45.35±3.9°), further supporting the prevalence of flatfoot (p = 0.000).

Radiographic analysis showed a markedly higher cuboid abduction angle (CAA) in the OA group (16.56±8.23°) versus controls (3.96±1.10°, p = 0.000), indicating midfoot pronation. However, the calcaneal pitch angle (CPA) did not show significant differences between the two groups (26.45±6.69° in OA vs. 23.61±4.09° in controls, p = 0.35).

Flatfoot prevalence was notably higher in the OA group, with 80% showing pronated foot based on arch index and 89% based on arch angle. A significant association was found between BMI and flatfoot status (χ^2 = 8.372, p = 0.004), while age and gender showed no statistically significant associations.

Correlation analysis indicated a significant negative correlation between arch index and truncated arch (r = -0.565, p < 0.001), Foot Posture Index (FPI) (r = -0.539, p < 0.001), and calcaneal pitch (r = -0.352, p = 0.018), whereas correlations involving arch angle were weak and non-significant.

Table 1. Characteristics of participants with and without medial knee osteoarthritis

Parameters	Without OA (n=33)	With OA (n=45)	p-value
Arch index	0.2427±.023	0.2813±.045	0.000
Arch angle	45.3515±3.9	30.9378±7.85	0.000
BMI	22.9697±2.7	30.4689±4.02	0.000
CP angle	23.6182±4.09	26.4467±6.69	0.35
CAA angle	3.9606±1.10	16.5578±8.23	0.000

Table 2. Distribution of characteristics by Arch Index and arch angle

Foot characterstics	Parameters	Frequency	Percent(%)
Pronated	Arh index	36	80
	Arch angle	40	89
Normal	Arh index	9	20
	Arch angle	5	11
Total	Arh index	45	100
	Arch angle	45	100

Table 3. Association of Arch Index with age, gender and BMI

Age	Arch Index		Chi square, p value
	Pronated	Normal	
less than 50	14(77.8)	4(22.2)	0.093, 0.761
≥50	22(81.5)	5(18.5)	
Gender			
Male	12(80.0)	3(20.0)	2.314, 0.789
Female	24(80.0)	6(20.0)	
BMI			
Normal	0(0.0)	2(100.0)	8.372, 0.004
Overweight	36(83.7)	7(16.3)	

Table 4. Association of Arch angle with age, gender and BMI

Age	Arch Angle		Chi square, p value
	Normal	Flat foot	
less than 50	3(16.7)	15(83.4)	1.228, 0.746
≥50	2(7.4)	25(92.6)	
Gender			
Male	1(6.7)	14(93.3)	0.750, 0.369
Female	2(6.7)	28(93.3)	
BMI			
Normal	0(0.0)	2(100.0)	0.742, 0.863
Overweight	5(11.6)	38(88.4)	

DISCUSSION

The present study aimed to investigate the relationship between pedographic (Arch index and Arch angle) and radiographic parameters (calcaneal pitch angle and cuboid abduction angle) of the foot in individuals with and without medial knee osteoarthritis (MKOA) in the Dehradun district. The results reveal significant differences in both arch index and arch angle between individuals with MKOA and those without, supporting the hypothesis that alterations in foot biomechanics—particularly a pronated foot posture—may be associated with knee osteoarthritis.

The arch index was significantly higher in participants with MKOA (0.2813±0.045) compared to those without (0.2427±.023), indicating flatter feet in the OA group. Correspondingly, the arch angle was significantly lower in the OA group (30.93±7.85°), further confirming the presence of foot pronation. These findings strongly suggest that the altered foot posture and reduced medial arch integrity may play a contributory role in the pathogenesis or progression of MKOA.

The study's outcomes align with the established understanding that foot biomechanics significantly impact the loading and kinematics of the knee joint. In the kinetic chain of the lower limb, the foot and knee function in tandem; excessive foot pronation has been shown to increase internal tibial rotation and medial knee compartment loading, both of which are implicated in the development and progression of MKOA.

This biomechanical interrelationship is consistent with earlier research by Guler et al. [3], Riskowski et al. [5], and Iijima et al. [11], all of whom identified a link between altered foot posture and increased knee pain and disability in OA patients. Moreover, the statistically significant association of BMI with both flatfoot prevalence and MKOA incidence ($p < 0.001$) in our study echoes findings by Menz et al. [15] and Rothrauff et al. [17], reinforcing the idea that obesity exacerbates mechanical loading on both the foot arch and knee joint, thus amplifying degenerative processes.

A further notable observation is the significant positive correlation between the arch index and cuboid abduction angle (CAA), which was markedly elevated in MKOA patients (16.55±8.23°) compared to controls (3.96±1.10°, $p < 0.001$). The CAA reflects midfoot abduction, which is a feature of excessive pronation. Increased CAA is indicative of midtarsal joint instability and transverse plane foot deformities—conditions that can alter the gait cycle and affect proximal joints like the knee. This observation aligns with Inui et al. [13], who documented a relationship between midfoot deformities and radiographic signs of knee OA, and supports the growing body of evidence suggesting that

foot abnormalities may not be mere consequences of OA-related disuse or aging but active contributors to pathological biomechanics.

The arch index was significantly higher in participants with MKOA (0.2813±0.045) compared to those without (0.2427±.023), indicating flatter feet in the OA group. Correspondingly, the arch angle was significantly lower in the OA group (30.93±7.85°), further confirming the presence of foot pronation. These findings strongly suggest that the altered foot posture and reduced medial arch integrity may play a contributory role in the pathogenesis or progression of MKOA.

The study's outcomes align with the established understanding that foot biomechanics significantly impact the loading and kinematics of the knee joint. In the kinetic chain of the lower limb, the foot and knee function in tandem; excessive foot pronation has been shown to increase internal tibial rotation and medial knee compartment loading, both of which are implicated in the development and progression of MKOA. This biomechanical interrelationship is consistent with earlier research by Guler et al. [3], Riskowski et al. [5], and Iijima et al. [11], all of whom identified a link between altered foot posture and increased knee pain and disability in OA patients. Moreover, the statistically significant association of BMI with both flatfoot prevalence and MKOA incidence ($p < 0.001$) in our study echoes findings by Menz et al. [15] and Rothrauff et al. [17], reinforcing the idea that obesity exacerbates mechanical loading on both the foot arch and knee joint, thus amplifying degenerative processes.

A further notable observation is the significant positive correlation between the arch index and cuboid abduction angle (CAA), which was markedly elevated in MKOA patients (16.55±8.23°) compared to controls (3.96±1.10°, $p < 0.001$). The CAA reflects midfoot abduction, which is a feature of excessive pronation. Increased CAA is indicative of midtarsal joint instability and transverse plane foot deformities—conditions that can alter the gait cycle and affect proximal joints like the knee. This observation aligns with Inui et al. [13], who documented a relationship between midfoot deformities and radiographic signs of knee OA, and supports the growing body of evidence suggesting that foot abnormalities may not be mere consequences of OA-related disuse or aging but active contributors to pathological biomechanics.

While the calcaneal pitch angle (CPA) was slightly elevated in the OA group (26.44±6.69°) compared to controls (23.61±4.09°), the difference was not statistically significant ($p = 0.35$). Interestingly, despite CPA being traditionally considered a marker of medial arch height, its variability in our sample may reflect compensatory

mechanisms, anatomical variations, or postural adaptations over time. These inconsistencies are not uncommon; Tayashiki et al. [16] and Kobayashi et al. [17] also reported varying levels of correlation between arch index and calcaneal pitch, suggesting that dynamic and static measurements of foot posture may not always align due to differences in weight-bearing status, muscular control, and joint laxity.

The findings on demographic associations are also instructive. The prevalence of flat feet and MKOA was found to be higher among individuals aged over 50 years, in females, and in overweight participants, although statistical significance was reached only in the BMI category ($p = 0.004$). These results are consistent with prior epidemiological studies such as those by Felson et al. [6] and Lawrence et al. [8], who documented a higher incidence of OA in older adults and females, attributing it to hormonal influences, reduced muscle mass, and joint alignment differences. The lack of statistically significant associations for age and gender in the current study may be due to sample size constraints, but the trends remain in agreement with broader literature and indicate the need for targeted screening in these high-risk groups.

Table 5. Arch index of pronated foot

S. No	Author	Population	Year	Mean ±sd
1	George S Murley et al[18]	Australian	2009	0.30 ± 0.07
2	Menz et al[15]	Australian	2010	028±0..05
3	Dwi Basuki Wibowo et al[19]	Indonesian	2017	0.543±0.057
4	Gunawan Dwi Haryadi et al[20]	Indonesian	2018	0.319 ± 0.040
5	Mr. Chandan Kumar Yadav et al[21]	Indian	2022	1.03 ± 0.1058
6	Present study	Indian	2024	0.2813±0.045

Table 6. Arch angle of pronated foot

S. No.	Author	Sample size	Population	Year	Mean±Sd
1	Patel M et al22	284	Indian	2021	29.00±3.87
2	Hegazy F et al23	460	UAE	2020	36.71±3.20
3	Pauk J et al24	42	USA	2014	24.1 ± 4.0
4	Zhang M et al 25	95	Chinese	2022	28.47±13.24
5	Present study	45	Indian	2024	30.9378±7.85

The clinical implication of this study is profound. Given the strong correlation between pedographic indicators and MKOA, particularly in resource-limited settings where radiography may not be readily available, pedography offers a viable, cost-effective screening tool. Arch index and arch angle measurements using the Harris mat provide rapid, non-invasive insights into foot biomechanics.

Their correlation with radiographic markers like cuboid abduction angle and, to a lesser extent, calcaneal pitch angle, enhances their utility in community-level screening programs. Furthermore, the ability to detect early foot malalignment and pronation can inform timely interventions, such as prescribing orthoses, footwear modifications, and physical therapy, thereby possibly delaying or mitigating the progression of MKOA.

In particular, the application of pedography could be pivotal in screening obese individuals, elderly populations, and pregnant women—all of whom are prone to altered gait mechanics and foot posture changes. Pregnancy, in particular, introduces ligamentous laxity and weight gain, both of which could contribute to medial arch collapse and subsequent knee malalignment. Although not directly studied here, extrapolating these findings to such populations opens avenues for preventive care strategies and targeted interventions.

Despite the strengths of the study, including its use of both pedographic and radiographic data and the relevance of its findings to an Indian population (where flatfoot prevalence and OA risk factors may be underdiagnosed), there are several limitations. The sample size, though adequate for preliminary conclusions, limits the statistical power to detect more subtle correlations, particularly in subgroup analyses. A larger, multicentric cohort study would be beneficial to confirm the associations observed. Moreover, the cross-sectional design restricts causal inference; while foot posture is associated with MKOA, it remains unclear whether the altered biomechanics precede the onset of osteoarthritis or are adaptive consequences thereof. Longitudinal studies would be instrumental in resolving this temporal ambiguity.

Another limitation pertains to the use of 2D pedography and plain radiography, which, although practical and economical, lack the depth and detail of 3D imaging or dynamic gait analysis. This restricts the ability to capture real-time changes in joint mechanics and muscular coordination, which are critical in comprehensively understanding the pathophysiology of MKOA. Future studies could incorporate plantar pressure mapping, motion capture systems, or weight-bearing CT/MRI for a more nuanced analysis. Additionally, while our study did not assess functional outcomes such as pain severity, walking speed, or quality of life, including

such parameters could strengthen the clinical relevance of biomechanical measurements.

In light of these findings, it is recommended that clinicians and public health practitioners consider integrating routine foot assessments—particularly arch index and arch angle evaluations—into OA screening protocols, especially in high-risk groups. Educational programs on proper footwear and the role of orthotic supports should be promoted in community health settings. Finally, future research should aim to explore the effectiveness of targeted foot interventions (such as custom orthotics or strength training for foot muscles) in reducing pain and improving function in MKOA patients.

Hence, this study highlights a significant association between flatfoot as characterized by elevated arch index and reduced arch angle, and the presence of medial knee osteoarthritis. These pedographic parameters, particularly when corroborated by radiographic features like increased cuboid abduction angle, offer valuable insight into the biomechanical factors contributing to MKOA. Pedography emerges as an accessible and effective tool in the early identification and potential prevention of knee osteoarthritis, particularly in resource-constrained environments. Further investigation with larger cohorts, dynamic biomechanical assessments, and interventional follow-up will be critical in fully harnessing the potential of foot-based screening and management strategies for knee osteoarthritis.

CONCLUSION

Arch index and arch angle in the Dehradun region were found to be 0.2813±0.045 and 30.9378±7.85. Regular assessments of pedographic parameters (arch index,arch and angle) can be beneficial in monitoring changes in foot structure, especially in populations at risk, specially in obese individuals. In remote areas where facility of x ray radiography is not available, measurement of the progression of osteoarthritis can be done with the help of pedographic parameters along with the progression of MKOA in pregnant women. The relationship between arch index, calcaneal pitch angle, and BMI underscores the importance of these parameters in understanding foot health and biomechanics. Pedography provides excellent visualization of the footprint and can be used as screening procedure for early identification of flat foot and other foot malalignment and its effective management by using orthotics.

REFERENCES

1. Poole AR, Guilak F, Abramson SB. Etiopathogenesis of osteoarthritis. In: Moskowitz RW, Altman RD, Buckwalter JA, Goldberg VM, editors. Osteoarthritis: Diagnosis and Medical/Surgical

Management. 4th ed. Philadelphia: WB Saunders; 2007. p. 27–49.

2. Kumar H, Pal CP, Sharma YK, Kumar S, Uppal A. Epidemiology of knee osteoarthritis using Kellgren and Lawrence scale in Indian population. J Clin Orthop Trauma. 2020 Feb;11(Suppl 1):S125–9.
3. Guler H, Karazincir S, Turhanoglu AD, Sahin G, Balci A, Ozer C. Effect of coexisting foot deformity on disability in women with knee osteoarthritis. J Am Podiatr Med Assoc. 2009 Jan;99(1):23–7.
4. Toda Y, Tsukimura N, Kato A. The effects of different elevations of laterally wedged insoles with subtalar strapping on medial compartment osteoarthritis of the knee. Arch Phys Med Rehabil. 2004 Apr;85(4):673–7.
5. Riskowski JL, Dufour AB, Hagedorn TJ, Hillstrom HJ, Casey VA, Hannan MT. Associations of foot posture and function to lower extremity pain: results from a population-based foot study. Arthritis Care Res (Hoboken). 2013 Nov;65(11):1804–12.
6. Felson DT, Lawrence RC, Dieppe PA, Hirsch R, Helmick CG, Jordan JM, et al. Osteoarthritis: new insights. Part 1: the disease and its risk factors. Ann Intern Med. 2000 Oct 17;133(8):635–46.
7. Kim JS, Lee MY. The effect of short foot exercise using visual feedback on the balance and accuracy of knee joint movement in subjects with flexible flatfoot. Medicine (Baltimore). 2020 Mar;99(13):e19260.
8. Lawrence RC, Helmick CG, Arnett FC, Deyo RA, Felson DT, Giannini EH, et al. Estimates of the prevalence of arthritis and selected musculoskeletal disorders in the United States. Arthritis Rheum. 1998 May;41(5):778–99.
9. Goodman SM, Springer B, Guyatt G, Abdel MP, Dasa V, George M. American College of Rheumatology/American Association of Hip and Knee Surgeons guideline for the perioperative management of antirheumatic medication in patients with rheumatic diseases undergoing elective total hip or total knee arthroplasty. Arthritis Rheumatol. 2017 Sep;69(8):1538–51.
10. Mochizuki T, Omori G, Nishino K, Tanaka M, Tanifuji O, Koga H, et al. The medial inclination of the proximal tibia is associated with the external knee adduction moment in advanced varus knee osteoarthritis. Knee Surg Sports Traumatol Arthrosc. 2022 Feb;30(2):574–83.
11. Iijima H, Ohi H, Isho T, Aoyama T, Fukutani N, Kaneda E, et al. Association of bilateral flat feet with knee pain and disability in patients with knee osteoarthritis: a cross-sectional study. J Orthop Res. 2017 Nov;35(11):2490–8.
12. Hawes MR, Nachbauer W, Sovak D, Nigg BM. Footprint parameters as a measure

of arch height. Foot Ankle. 1992 Jan;13(1):22–6.

13. Inui K, Ikoma K, Imai K, Ohashi S, Maki M, Kido M, et al. Examination of the correlation between foot morphology measurements using pedography and radiographic measurements. J Foot Ankle Surg. 2017 Mar;56(2):298–303.
14. Gentili A, Masih S, Yao L, Seeger LL. Foot axes and angles. Br J Radiol. 1996 Oct;69(826):968–74.
15. Menz HB, Sherrington C. Foot posture and foot function in older people: a review of the literature. J Aging Res. 2006;2006:35884.
16. Tayashiki K, Yamada K, Yamamoto S. Correlation between arch index and calcaneal pitch angle in healthy adults. J Phys Ther Sci. 2014 Mar;26(3):433–6.
17. Kobayashi K, Yamada K, Yoshimoto H. The relationship between foot arch index and calcaneal pitch angle in various foot types. J Foot Ankle Res. 2018 Jan;11(1):5.
18. Rothrauff BB, Miller MC, de Meireles SM, et al. The influence of obesity on foot biomechanics: a systematic review. J Foot Ankle Surg. 2016 Jul–Aug;55(4):855–64.
19. Wibowo DB, Haryadi GD, Widodo A, Rahayu SP. Correlation of loaded and unloaded foot area with arch index in younger flatfoot. MATEC Web Conf. 2017;135:00060.
20. Haryadi GD, Wibowo DB, Widodo A, Suprihanto A. Comparison of ratio loaded and unloaded foot area of flat foot and healthy foot in younger adults. MATEC Web Conf. 2018;159:02019.
21. Yadav CK, Modi V, Rani A, Rajput K, Mishra R, Srivastava S. A study on prevalence of flat foot among children 5–10 years and adults above 18 years in Lucknow population: a cross-sectional study. NeuroQuantology. 2022;20(15):3127.
22. Patel M, Shah P, Ravaliya S, Patel M. Relationship of anterior knee pain and flat foot: a cross-sectional study. Int J Health Sci Res. 2021;11(3):86–92.
23. Hegazy F, Aboelnasr E, Abuzaid M, Kim IJ, Salem Y. Comparing validity and diagnostic accuracy of Clarke's angle and foot posture index-6 to determine flexible flatfoot in adolescents: a cross-sectional investigation. J Multidiscip Healthc. 2021 Sep 27;14:2705–17.
24. Pauk J, Ihnatouski M, Najafi B. Assessing plantar pressure distribution in children with flatfoot arch: application of the Clarke angle. J Am Podiatr Med Assoc. 2014 Nov;104(6):622–32.
25. Zhang M, Nie MD, Qi XZ, Ke S, Li JW, Shui YY, et al. A strong correlation between the severity of flatfoot and symptoms of knee osteoarthritis in 95 patients. Front Surg. 2022 Jun 30;9:936720.

https://doi.org/10.46351/jas.v32i2pp66-77

JAS Journal of Anatomical Sciences (U.P. Chapter of Anatomical Society of India)

Original Article

Morphometric analysis of dried skulls for optimization of transorbital approaches to middle cranial fossa: Anatomic insights for surgical planning

Deepika Poonia[1], Srishty Raman[1], Shubhi Saini[1], Sabita Mishra[1]

1. Department of Anatomy, Maulana Azad Medical College, New Delhi, India

ABSTRACT

Introduction: The structures in the middle cranial fossa are challenging to assess due to complex placement and relations. Recent advances like transorbital approach offers a direct route to cranial targets via the orbit, reducing manipulation of neurovascular structures and improving postoperative outcomes. However, there is limited data on distances between orbital rim landmarks and key cranial structures. This study aims to provide critical quantitative data to support precise intracranial navigation.

Materials and Methods: The study analyzed 43 human skulls of unknown age and sex. Linear distances from the superolateral angle and supraorbital notch of the orbital rim to key landmarks in the middle cranial fossa were measured using ImageJ software. Linear distance of important landmarks pertaining to transorbital approach from lateral orbital rim were recorded. Data was statistical analyzed using GraphPad Prima 8.0.2.

Results: All the linear distances obtained between the key landmarks in middle cranial fossa like trigeminal fossa, foramen ovale, spinosum and rotundum; carotid sulcus upto supraorbital notch were less then those obtained from frontozygomatic suture. Bilaterally structures showed consistency (Student's t-test, $p = 0.6624$).

Conclusions: This study provides precise, reproducible measurements that can guide surgeons in locating critical middle cranial landmarks for safe navigation into the orbital and cranial cavity during transorbital neuroendoscopic surgeries. These findings will be valuable for both anatomical education and neurosurgical practice.

Keywords: Trigeminal fossa, Carotid sulcus, Foramen ovale, Foramen spinosum, Foramen rotundum, ImageJ

Address for Correspondence:
Dr. Deepika Poonia, Assistant Professor, Department of Anatomy, Maulana Azad Medical College, New Delhi, India
Email: dr.deepikapoonia@gmail.com Mob.: 8285048497

Date of Receiving: 27 Aug 2024
Date of Acceptance: 29 Sep 2024

INTRODUCTION

The middle cranial fossa is a complex space which houses several important neurovascular structures which are placed in intricate relation to each other [1]. These neurovascular structures may get susceptible to pathologies, tumours and congenital anomalies making this area clinically significant. However complex placement of these structures, makes it challenging for the neurosurgeons and interventional radiologists to navigate towards their target through this cavity [1, 2]. Following popularization of endoscopic approach, several routes (transnasal, supraorbital and transorbital) have been defined to assess structures present over central skull base. Endoscopic transorbital approach offers a direct and minimally invasive approach to targets in orbit and middle cranial fossa. It was first defined by Mois in 2010 and has recently gained notoriety amongst neurosurgeons [3].

Anatomically, middle cranial fossa is divided into sellar and parasellar portions. Sellar region contains pituitary gland resting on sella turcica [1]. The parasellar region comprises of critical neurovascular structures like cavernous sinus, internal carotid artery, cranial nerves, meckle's cave with Gasserian ganglion along with V1, V2, V3 branches and middle meningeal artery. Endoscopic transorbital approach offers a narrow and safe corridor to address small lesions in parasellar and lateral part of middle cranial fossa [4].

The cavernous venous sinus is highly vulnerable space. Several cranial nerves (oculomotor, trochlear, ophthalmic, abducent) and internal carotid artery are contained in the wall and cavity of cavernous sinus. Tumor, congenital anomaly, infection and vascular pathology like carotidocavernous fistula and carotid aneursym may involve one or more compartments of cavernous sinus. Endoscopic transorbital route offers a promising approach to expose all the regions (Dolenc's/Clinoid triangle, supratrochlear triangle, Parkinson's/infratrochlear triangle, Mullan's /anteromedial triangle, anterolateral triangle) defined except Hakuba/oculomotor triangle which needs transnasal approach. Also, transorbital corridor provides a safer route to assess carotid aneurysm in the paraclinoid part of internal carotid artery for surgical clipping [2]. When transvenous endovascular embolisation via facial vein or inferior petrosal sinus is challenging then transorbital endoscopic approach provides an alternate surgical approach to obliterate these carotidocavernous fistula [5].

In past few decades, transorbital neuroendoscopic surgical (TONES) approach has gained popularity. It has opened a safe and minimally invasive corridor to expose structures present in anterolateral aspect of middle cranial fossa i.e. parasellar and lateral aspect of cranial cavity up to petrous temporal bone which cannot be reached by endonasal approach [6]. In transorbital approach, upper eyelid crease curvilinear skin incision is

placed to identify orbital septum and to create surgical plane deep to orbicularis oculi.

On reaching orbital rim, periorbita is elevated to navigate antero-posteriorly inside the orbital cavity. During endoscopic approach the lateral wall of orbital cavity displays two important anatomical landmarks. One is consistently seen in all skulls- frontosphenoid suture, the key landmark to decide the site of bone drilling beyond which dissection continues in a plane deep to periorbita till the lateral margin of superior orbital fissure (SOF) & inferior orbital fissure (IOF) is identified [7]. Second landmark is meningo-orbital foramen [8]. Several names attributed to meningo-orbital foramen are- craniorbital foramen, lacrimal foramen, foramen of Hyrtl, sphenofrontal foramen, sinus canal foramen and anastomotic foramen [9].

The meningo-orbital/ orbito-lacrimal artery may be the orbital branch of middle meningeal artery or anastomosis between the orbital branch of middle meningeal artery and lacrimal artery [10]. This foramen is an inconstant but important landmark for SOF & IOF. The meningo-orbital vessels are potential source of significant haemorrhage hence mandates careful dissection of lateral orbital wall. This reflects the significance of knowing prevalence and anatomical details of this foramen [8]. Intraorbital part of greater wing of sphenoid is drilled to expose temporal dura. Interperiosteal dural dissection via meningo-orbital band to reach lateral wall of cavernous sinus and Gasserian ganglion is done. Middle meningeal artery supplying duramater is cut to prevent the intraoperative haemorrhage.

Despite the plethora of work done to describe different ways to transorbitally approach middle cranial fossa, there is a paucity of reports providing quantitative data to be used to carefully navigate through orbit to reach targets in middle cranial fossa. Hence the aim of current study was to provide quantitative anatomical data from orbital rim to paramedian and lateral structures in middle cranial fossa. The study also provides data of important landmarks in lateral wall of orbital cavity. Any anatomical variation in the route may create dilemma during surgery, hence awareness about the possible bony and vascular variations is important.

MATERIAL AND METHODS

A cross-sectional survey was conducted on 43 dry human skulls (without calvaria or cranium) of unknown age and sex, sourced from the Department of Anatomy, Maulana Azad Medical College (MAMC), New Delhi.

Sample size was calculated using the equation n= (Z1−α/22 p(1−p))/ d2

where n is the estimated sample size, Z1−α/2 is the standard normal variate (at a 5% type I error (P < 0.05), it's value 1.96), p represents

the expected population proportion from previous or pilot studies, and d is the absolute error or precision (set at 20%, i.e., d=0.2) [11]. As the study is novel and lacks prior data on morphometric dry skull measurements of the middle cranial cavity landmarks relative to the orbit, p was set to 0.5 to yield the largest sample size for a given d [12]. This calculation determined a minimum sample size of 24 skulls, and thus 43 intact skulls were included. Skulls with damage or deformation at the skull base or orbital cavity were excluded from analysis.

Each skull was numbered, and key landmarks relative to the orbital rim-supraorbital notch and frontozygomatic suture were identified and marked. Vertical lines were traced onto the cranium's outer table with chalk to map these landmarks in the norma verticalis cranii plane. Skulls were aligned in Frankfurt's plane and photographed from a superior (norma verticalis) view, with the camera positioned at a fixed distance and a 90° angle to the skull base. Using NIH ImageJ software, digital linear measurements were taken for distances between the two external landmarks- supraorbital notch and frontozygomatic suture and key anatomical points, which included (Fig. 1):

A. Carotidoclinoid notch
B. Medial end of trigeminal fossa
C. Lateral end of trigeminal fossa
D. Anterior borders of foramina ovale
E. Anterior borders of Foramen rotundum
F. Anterior borders of Foramen spinosum
G. Apex of the petrous part of the temporal bone
H. Posterior clinoid process
I. Midpoint of the carotid sulcus

Additionally, variations in orbital morphology relevant to the TONES approach, such as meningo-orbital foramina was also documented. Specifically, the prevalence, number, and location of the meningo-orbital foramen were recorded. Considering the surgical importance of the frontosphenoid suture and meningo-orbital artery, their distances from the superolateral orbital rim margin were measured using a divider and ruler [13-15]. To minimize intraobserver variability, all measurements were taken independently by two co-authors, with mean values used for analysis.

Intra-rater Reliability Test: To assess operator reliability, measurements were repeated on a randomly selected skull three times across seven sessions, and the coefficient of variance was calculated.

Statistical Analysis: Data were analyzed using GraphPad Prism 8.0.2. Descriptive statistics (mean, range, standard deviation) were calculated. The Kolmogorov-Smirnov test was used to test the normality assumption. The two-tailed independent sample t-test was performed to compare means between

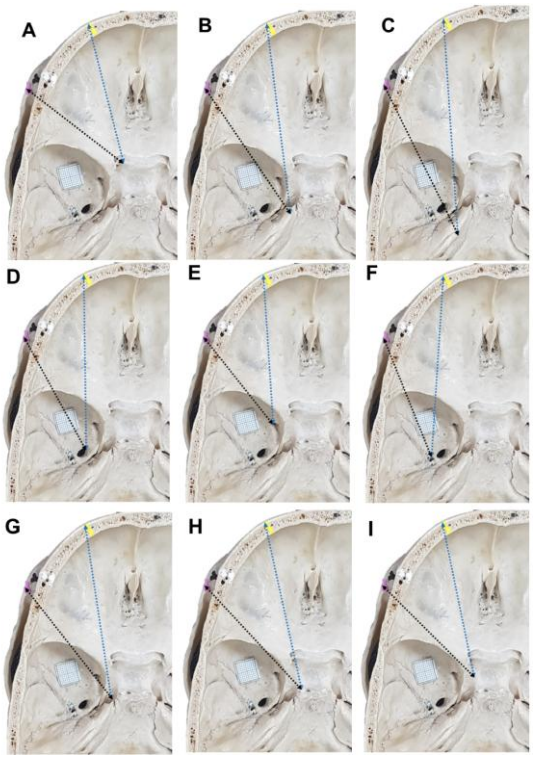

Fig. 1. Photograph of superior view of cranial cavity showing, linear distance between external orbital landmarks – Supraorbital foramen and Frontozygomatic suture (marked with yellow and pink chalk, respectively) and intracranial key targets- (A) carotidoclinoid notch, (B) medial and (C) lateral trigeminal fossa margins, (D) anterior borders of foramina ovale, (E) rotundum and (F) spinosum, (G) apex of petrous part of temporal bone, (H) posterior clinoid process, and (I) midpoint of carotid sulcus measured from supraorbital foramen (marked with blue-colored arrow) and frontozygomatic suture (marked with black-colored arrow), respectively.

groups. P < 0.05 was considered to be statistically significant.

RESULTS

The range, mean, and standard deviation of each middle cranial cavity anatomical point evaluated from supraorbital foramen and frontozygomatic suture, respectively on the right and left sides are summarized in Table 1. We found no significant differences in laterality in any of the measurements (P < 0.05).

The average of the measurements of the middle cranial cavity landmarks from the frontozygomatic suture were significantly shorter than those from the supraorbital foramen, indicating a more direct approach route to cranial cavity structures (Fig. 2).

Distance of Frontosphenoid suture from Frontozygomatic suture:

The frontosphenoid suture on the lateral orbital wall, along with the meningo-orbital foramina, serves as critical landmarks for surgeons during the TONES approach. Descriptive statistics for frontosphenoid suture location relative to the frontozygomatic suture are presented in Table 2, showing no significant side-to-side difference.

Meningo-orbital foramen:

The meningo-orbital foramen was present in 55% of skulls (24 out of 43), with approximately 60% located in the frontal bone and the remaining 40% in the sphenoid bone. Among these 24 skulls, 15 exhibited a bilateral presentation, while 9 showed a unilateral presence of the foramen within the orbit. A small subset (~5%) displayed duplication of the foramen. Table 3 presents descriptive statistics of the frontosphenoid suture in relation to the frontozygomatic suture, showing no significant variation between sides.

DISCUSSION

The data obtained in this study provides a comprehensive analysis of the landmarks pertaining to the transorbital endoscopic approach to orbit and middle cranial fossa. There is paucity of information in literature which led authors to undertake this study. To discuss how the findings of present study relate to previous studies, presents a problem, as after thorough review of literature authors could not find a study to compare all the data obtained. We have thereafter compared the results with those of orbital studies.

The literature review unfolded previous anatomical morphometric analysis done in axial plane using CT-Scan, to measure the angular distance between the vectors extending from frontozygomatic suture and four target points- tip of anterior clinoid process, foramen ovale, foramen rotundum and lateral margin of trigmenial fossa [16].

Other studies have measured the area of anterolateral triangles on central skull base to expose vivian canal and its contents [17].

Despite the growing importance of transorbital endoscopic approach to paramedian and lateral structures in middle cranial fossa, there is lack of work done to measure the linear distance between orbital rim and key structures in middle cranial fossa. Present study provides data pertaining to the distance of external landmark to intracranial bony target. No difference was found on comparing data of both sides. However, all the distances measured from supraorbital notch located medially were higher than frontozygomatic suture located laterally. This suggests the lateral orbital wall provides shorter route for navigation.

Frontosphenoid suture and Meningo-orbital foramen

The frontosphenoid suture and meningo-orbital artery are essential landmarks in the TONES approach, helping surgeons safely navigate the lateral orbital wall. Measurements of their distances from the superolateral orbital rim margin provide reliable markers, guiding precise positioning within the orbit to avoid damage to critical structures.

Table 1. Key middle cranial cavity anatomical landmarks measurements from supraorbital foramen and frontozygomatic suture, respectively

Distance from		SUPRAORBITAL FORAMEN			FRONTOZYGOMATIC SUTURE		
Cranial cavity landmarks	Side	Range (cm)	Mean ± SD (cm)	p-value	Range (cm)	Mean ± SD (cm)	p-value
Carotidoclinoid notch	Right	6.69-8.94	7.45± 0.55	0.73	4.60-6.52	5.91± 0.39	0.98
	Left	6.26-8.65	7.41± 0.60		5.23-6.66	5.92± 0.33	
Medial margin of Trigeminal fossa	Right	8.65-11.49	9.76± 0.66	0.76	6.47-8.46	7.37± 0.44	0.82
	Left	8.63-11.11	9.71± 0.68		6.36-8.46	7.35± 0.41	
Lateral margin of Trigeminal fossa	Right	9.16-12.02	10.39± 0.69	0.5462	6.81-8.71	7.65± 0.45	0.32
	Left	9.07-12.01	10.30± 0.71		6.36-8.87	7.55± 0.48	
Anterior border of foramen ovale	Right	7.58-10.32	8.81± 0.68	0.59	5.33-6.99	5.95± 0.38	0.75
	Left	7.68-10.21	8.73± 0.68		5.12-7.01	5.98± 0.39	
Anterior border of foramen rotundum	Right	6.35-8.99	7.54± 0.65	0.80	4.10-5.87	4.99± 0.38	0.17
	Left	6.13-8.88	7.50± 0.66		3.92-5.83	5.11± 0.38	
Anterior border of foramen spinosum	Right	8.08-11.07	9.39± 0.72	0.45	5.79-7.29	6.15± 0.45	0.99
	Left	8.14-10.78	9.27± 0.70		5.21-7.58	6.15± 0.44	
Apex of petrous part of temporal bone	Right	8.45-11.21	9.44± 0.65	0.67	6.43-8.06	7.24± 0.39	0.88
	Left	8.15-10.86	9.37± 0.67		6.39-8.19	7.25± 0.36	
Posterior clenoid process	Right	8.08-10.18	8.99± 0.57	0.89	6.34-7.94	7.18± 0.40	0.41
	Left	7.91-10.39	8.97± 0.62		6.41-8.46	7.25± 0.39	
Midpoint of carotid sulcus	Right	7.61-9.79	8.39± 0.59	0.92	5.84-7.52	6.65± 0.36	0.41
	Left	7.44-9.68	8.41± 0.59		5.92-7.46	6.71± 0.37	

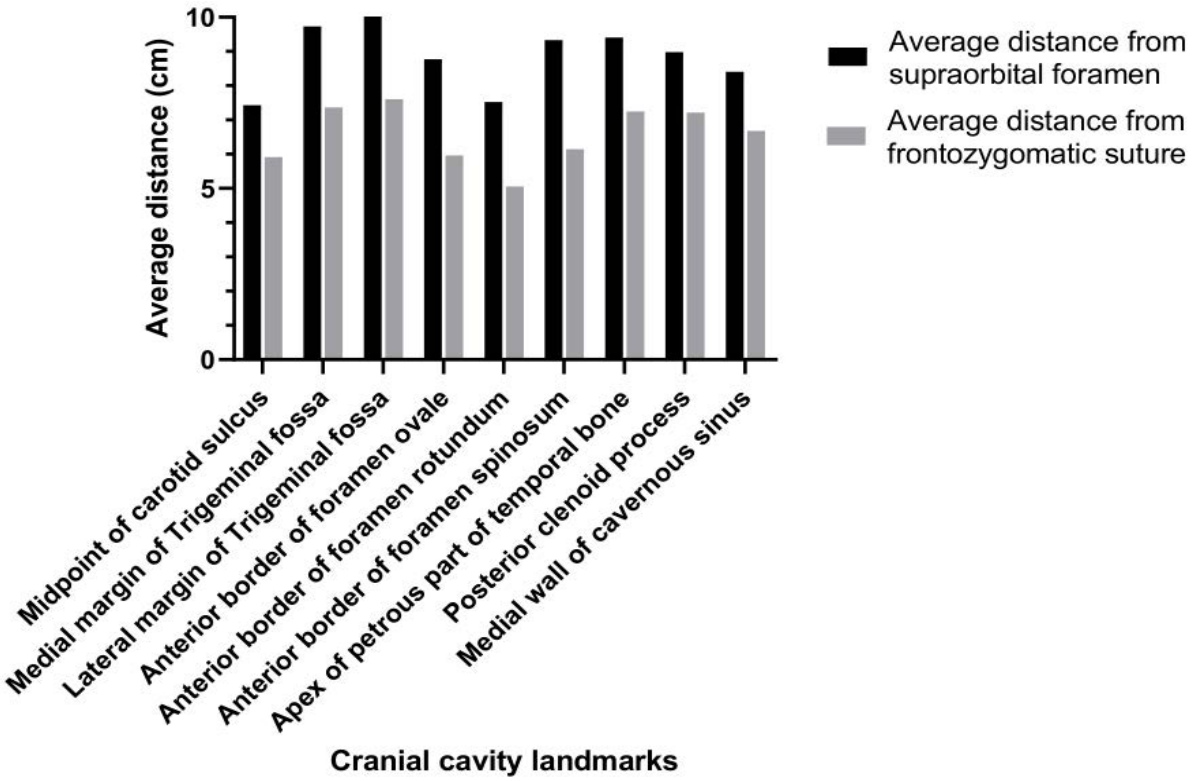

Fig. 2. Comparison of the average distances from the supraorbital foramen and frontozygomatic suture to the middle cranial cavity landmarks.

Table 2. Position of the frontosphenoid suture with respect to the frontozygomatic suture

Side	Range (cm)	Mean ± SD (cm)	p-value
Right	0.95- 2.10	1.458 ± 0.3	0.1213
Left	0.60- 2.0	1.356 ± 0.3	

Table 3. Position of the meningo-orbital foramen with respect to the frontozygomatic suture

Side	Range (cm)	Mean ± SD (cm)	p-value
Right	2.00- 3.07	2.885 ± 0.6	0.1332
Left	2.00- 2.92	2.622 ± 0.3	

Table 4. Prevalence and location of meningo-orbital foramen in the orbits of dry skulls

Authors	Year	Ethnicity	Sample size	Unilateral/ Bilateral	Prevalence	Location	Distance from fronto-zygomatic suture
Mahajan M et al [18]	2020	Asian (India)	223 skulls	Bilateral= 46.63% Unilateral= 53.37%	69.05%	-	24.9 ± 3.4mm
Macchi V et al [19]	2015	Siena	920 skulls	Bilateral= Nil Unilateral= 42.21%	42.21%	Frontal bone=58.26% Greater wing of sphenoid= 17.19% F-S suture=24.55%	-
Agarwal C et al [20]	2015	Asian (India)	42 skulls	Bilateral= Nil Unilateral= 42.24%	45.24%	-	-
Celik S et al [21]	2014	Europe (Turkey)	150 orbits of skulls	Bilateral= 52.4% Unilateral= 32.5%	84%		26.3 ± 3.9mm
O'Brien & McDonald [10]	2007	Europe (UK)			73%	Fronto-sphenoid suture	
Present study	2024	Asian (India)	43 skulls	Bilateral=62.5% Unilateral= 37.5%	45%	Frontal bone=60% Sphenoid bone=40%	27.52 ± 45

The mean distances from the frontozygomatic suture to the frontosphenoid suture on the right and left sides (1.458 ± 0.3 cm and 1.356 ± 0.3 cm, respectively) showed no statistically significant side-to-side variation. This symmetry is advantageous for surgical planning, as it allows surgeons to use a consistent reference point when approaching either side of the skull. These findings, detailed in Table 2, highlight the frontosphenoid suture as a dependable landmark, with a relatively

narrow range that facilitates accurate, side-independent orientation during TONES.

The meningo-orbital foramen is inconstant landmark during TONES but mandates careful navigation to avoid rupture followed by inevitable hemorrhage and blurring of surgical field. Previous studies have reported variable number and location of meningo-orbital foramen (Table 4).

The minimally invasive TONES approach provides an anterolateral entry to the middle cranial fossa through the lateral orbital wall, necessitating a thorough understanding of the prevalence and distribution of sutural bones, or wormian bones, in this region. Awareness of these sutural bones is crucial, as their displacement during surgery could result in damage to surrounding structures [22]. The lateral wall of the orbit, the thickest of all orbital walls, has a triangular shape and is formed by the orbital surface of the greater wing of the sphenoid posteriorly and the orbital surface of the frontal process of the zygomatic bone anteriorly. This wall is intersected horizontally near the roof by the frontal-sphenoid and frontal-zygomatic sutures, and vertically by the sphenoid-zygomatic suture [23].

CONCLUSION

This study provides valuable morphometric data essential for optimizing the transorbital endoscopic approach to the middle cranial fossa. By mapping precise distances from key orbital rim landmarks to significant cranial structures, these findings enable more accurate surgical navigation, thereby reducing intraoperative risks to critical neurovascular structures.

The presence of wormian bones in the lateral orbital wall and variations in meningo-orbital foramen prevalence highlight the need for individualized surgical planning to anticipate anatomical variations. This quantitative insight enhances anatomical education and surgical planning, supporting safer, minimally invasive approaches to the middle cranial fossa, especially in cases requiring access to parasellar and lateral skull base regions. Further studies correlating these findings with clinical outcomes could solidify the transorbital approach as a preferred method for specific neurovascular interventions.

REFERENCES

1. Letchuman V, Acosta N. Anatomy, Head and Neck, Middle Cranial Fossa. In: Treasure Island (FL): StatPearls Publishing; 2023.
2. Corvino S, Villanueva-Solórzano PL, Offi M, Armocida D, Nonaka M, Iaconetta G, Esposito F, Cavallo LM, de Notaris M. A New Perspective on the Cavernous Sinus as Seen through Multiple Surgical Corridors: Anatomical Study Comparing the Transorbital, Endonasal, and Transcranial Routes and the Relative Coterminous Spatial Regions. Brain Sci. 2023;13:1215.

3. Moe K, Ellenbogen RG. Transorbital Neuroendoscopic Surgery. Oper Neurosurg. 2010;67:ons16–ons28.
4. Standring S. Gray's Anatomy: The Anatomical Basis of Clinical Practice. Amsterdam: Elsevier; 2020.
5. Chen CJ, Caruso JP, Ding D, Schmitt PJ, Buell TJ, Raper DM, Evans A, Newman SA, Jensen ME. Transorbital Approach for Endovascular Occlusion of Carotid-Cavernous Fistulas: Technical Note and Review of the Literature. Cureus. 2017;9(1):e976.
6. Vural A, Ferrari M, Rampinelli V, Schreiber A, Mattavelli D, Doglietto F, Buffoli B, Rodella LF, Taboni S, Tomasoni M, Gualtieri T, Deganello A, Hirtler L, Nicolai P. Transorbital Endoscopic Approaches to the Skull Base: A Systematic Literature Review and Anatomical Description. Neurosurg Rev. 2021;44(5):2857-2878.
7. Nannavecchia BA, Cebula H, Scibilia A, Bozzi MT, Zaed I, Gallinaro P, Boujan F, Dietemann JL, Djennaoui I, Debry C, Ligarotti GKI, Signorelli F, Proust F, Chibbaro S. Endoscopic Transorbital Approaches to Anterior and Middle Cranial Fossa: A Laboratory Investigation on Surgical Anatomy and Potential Routes. J Neurol Surg. 2021;82(B4).
8. Zoia C, Solarii D, de Notaris M, Corrivetti F, Spena G, Cavallo LM. Transorbital and Supraorbital Uniportal Multicorridor Approach to the Orbit, Anterior, Middle, and Posterior Cranial Fossa: Anatomic Study. Brain Spine. 2024;4:102719.
9. Erturk M, Govsa F, Koc K, et al. The Cranio-Orbital Foramen, the Groove on the Lateral Wall of the Human Orbit, and the Orbital Branch of the Middle Meningeal Artery. Clin Anat. 2005;18(1):10-14.
10. O'Brien AM, Smith MS. The Meningo-Orbital Foramen in a Scottish Population. Clin Anat. 2007;20(8):880–885.
11. Charan J, Thakur B. How to Calculate Sample Size for Different Study Designs in Medical Research? Indian J Psychol Med. 2013;35(2):121-126.
12. U.S. Centers for Disease Control and Prevention. Micronutrient Survey Manual & Toolkit. International, N, editor. 2022.
13. Di Somma A, Cavallo LM, de Notaris M, Dallan I, Solari D, Zimmer LA, Keller JT, Zuccarello M, Prats-Galino A, et al. Endoscopic Transorbital Superior Eyelid Approach: Anatomical Study from a Neurosurgical Perspective. J Neurosurg. 2018;129:1203–1216.
14. Chibbaro S, Montano GM, Scibilia A, Todeschi J, Zaed I, Bozzi MT, Ollivier I, Cebula H, Santin MDN, Djennaoui I, et al. Endoscopic Transorbital Approaches to Anterior and Middle Cranial Fossa: Exploring the Potentialities of a Modified Lateral Retrocanthal Approach. World Neurosurg. 2021;150:e74–e80.
15. Serioli S, Nardi M, Plou P, De Bonis A,

Meyer J, Leonel LCPC, Tooley AA, Wagner LH, Bradley EA, Van Gompel JJ, Benini ME, Dallan I, Peris-Celda M. Surgical Anatomy of the Microscopic and Endoscopic Transorbital Approach to the Middle Fossa and Cavernous Sinus: Anatomo-Radiological Study with Clinical Applications. Cancers (Basel). 2023;15(18):4435.

16. Corvino S, Alessi KA, Piazza A, Corrivetti F, Spiriev T, Colamaria A, Cirrottola G, Cavaliere C, Esposito F, Cavallo LM, Iaconetta G, de Notaris M. Open-Door Extended Endoscopic Transorbital Technique to the Paramedian Anterior and Middle Cranial Fossae: Technical Notes, Anatomomorphometric Quantitative Analysis, and Illustrative Case. Neurosurg Focus. 2024;56(4):E7.
17. Corvino S, Armocida D, Offi M, et al. The Anterolateral Triangle as Window on the Foramen Lacerum from Transorbital Corridor: Anatomical Study and Technical Nuances. Acta Neurochir. 2023;165:2407–2419.
18. Mahajan M, Agarwal AA, Devi G, et al. Clinical Implications in Orbital and Pterional Flap Surgeries as Well as Radioimaging Studies to Determine Topographical Prevalence and Characterization of Meningo-Orbital Foramen in Orbits of the Indian Population. Int J Morphol. 2020;38(6):1810–1817.
19. Macchi V, Regoli M, Bracco S, et al. Clinical Anatomy of the Orbitomeningeal Foramina: Variational Anatomy of the Canals Connecting the Orbit with the Cranial Cavity. Surg Radiol Anat. 2016;38:165–177.
20. Agarwal C, Garg R, Kumar S, Sharma D, Pareek P. Foramen Meningo-Orbitale: Its Incidence and Clinical Significance in Indians. Indian J Basic Appl Med Res. 2015;4(4):127–132.
21. Celik S, Koc Z, Ozer MA, et al. Navigational Area of the Cranio-Orbital Foramen and Its Significance in Orbital Surgery. Surg Radiol Anat. 2014;36(10):981–988.
22. Mahajan R, Verma A, Tiwari S. Morphometric Study of Sutural Bones of Orbit with Their Clinical Implications. Int J Clin Exp Med Res. 2018;2(2):29-36.
23. Manjunath KY. Supernumerary Bones in the Walls of the Bony Orbit. People's J Sci Res. 2013;6(1).

https://doi.org/10.46351/jas.v32i2pp78-87

JAS Journal of Anatomical Sciences (U.P. Chapter of Anatomical Society of India)

Original Article

Exploring spinal geometry: The significance of Cobb's and Ferguson's angles in low back pain patients

Abhinav Kumar[1], Jolly Agarwal[1], Abhishek Chawdhery[1], Chandra Shekhar[1], Avantika Ramola[1], Mahendra Kumar Pant[1]

1. Department of Anatomy, Government Doon Medical College, Dehradun, India

ABSTRACT

Introduction: The vertebral column consists of vertebrae connected by interbody joints, facet joints, ligaments, and muscles. Evolutionarily lumbosacral angle appears to have developed with erect posture and bipedal locomotion. Lumbar Lordosis (LL) is the curvature of the lumbar spine, measured by Cobb's method, measured between L1 cranial endplate and S1 cranial endplate. Lumbosacral angle/Ferguson's angle, is the angle between the plane of the superior margin of S1 vertebrae and a horizontal line. This study aimed to measure Cobb's Angle and Ferguson's Angle on MRI Images (T2w) in patients with low back pain.

Materials and Methods: In the present study, MRI images (T2w) of total 210 patients (92 males & 118 females) suffering with low back pain were taken via Autocad software and measurements of Cobb's and Ferguson's angles were taken.

Results: Of the total samples, mean Cobb's angle was 44.60° ± 11.390° and mean Ferguson's angle was 37.63° ± 8.027°, showing a statistically significant strong positive correlation ($r = 0.925$, $p < 0.001$). Both males and females had significant positive correlations between Cobb's and Ferguson's angles ($p < 0.001$ in both and $r = 0.927$ in males and $r = 0.931$ in females). In males, there was a statistically significant correlation between Likert pain scale and both Cobb's angle ($p = 0.008$) and Ferguson's angle ($p = 0.005$), in females only Cobb's angle correlated with pain ($p = 0.019$).

Conclusions: This study concluded that with increasing pain both the Cobb's and Ferguson's angles increase. Both angles also tend to increase with advancing age. Measurement of these angles will be helpful in targeted assessment and interventional strategies for low back pain.

Keywords: Cobb's angle, Ferguson's angle, Low back pain, Lumbosacral angle

Address for Correspondence:
Dr. Abhinav Kumar, Junior Resident, Department of Anatomy, Government Doon Medical College, Dehradun, India
Email: rkabhinav.ak@gmail.com Mob.: 7017128505

Date of Receiving: 19 Sep 2024
Date of Acceptance: 27 Oct 2024

INTRODUCTION

Vertebral column is a curved linkage of individual vertebrae with cartilaginous interbody joints and paired synovial facet (zygapophysial) joints, and a complex of ligaments and overlying muscles and fasciae. It undergoes dynamic forces of everyday life, like compression, traction and shear, which can vary in magnitude and are influenced by occupation, posture and locomotion. There are total 5 lumbar vertebrae and 5 sacral vertebrae, contributing to about 12% and 8% of total body length respectively [1].

During development, vertebral column has primary thoracic and pelvic curves (dorsally convex), followed by appearance of secondary cervical and lumbar spinal curvatures in sagittal plane. In eighth week, lumbar flattening is also seen. After birth, slight sacral curvature is seen followed by influence of functional changes like head support, upright sitting, and walking leading to development of secondary curvatures in vertebral column and changes in the proportional size of vertebrae, especially in lumbar region.

This secondary lumbar curvature (lordosis) becomes important in maintaining the centre of gravity of the trunk over the legs when walking starts. The human lumbar spine is being labelled as "the evolutionary weak point" of the spine and is the commonest site for degenerative changes. Junction of L5-S1 vertebrae is the spinal segment with greatest individual curvature and about 20% of degenerative changes out of total spine occurs in this segment. The configuration of human lumbar spine is adapted throughout evolution [1].

Evolutionarily lumbosacral angle appears to be developed due to progressive acquisition of erect posture and development of bipedal locomotion and is related neither to age, height, weight nor obstetrical requirement (Maurice Abibtol). Normal angles for Lumbar lordosis is 20 degrees to 45 degrees. (Tuzun), and lumbosacral angle is 32° to 44° [2].

Lumbar Lordosis (LL) is defined as the curvature of the lumbar spine, it is unique to human spine & is necessary to facilitate upright posture (bipedalism). Wedging of vertebral bodies (50) contribute to approximately 10% of lumbar curve, while wedging of the discs (460) contributes the rest (90%). For balancing in the upright posture lumbar lordosis is essential and the developmental stages of bipedalism develops lordotic curve. The degree of lumbar lordosis is the main factor influencing the conversion of extensor power developed by the intrinsic back muscles to axial torsion necessary to rotate the pelvis during walking [3].

This curvature is critical for biomechanical stability in the lumbar region. It contributes to both the load bearing capacity and flexibility of the lumbar spine, which are important for activities of daily life. (Bailey) Lumbar lordotic

angle is measured by Cobb's method, measured between L1 cranial endplate and S1 cranial endplate [4].

Lumbosacral angle also known as sacro-horizontal angle/sacral angle/Ferguson's angle, is defined as the angle formed between a line across the plane of the superior margin of S1 vertebrae and a horizontal line. An increase in this angle suggests a mechanical factor in producing low back pain by increasing the shearing and compressive forces on the articular facets at the lumbosacral junction [2].

Low back pain (LBP) is a common symptom/complaint now a days, and is linked mainly to postal imbalances, causing joint stress and spraining of muscles and ligaments, excessive mechanical loading of tissues [5].

LBP is defined as pain with discomfort which is localized above the inferior gluteal folds and below the costal margin, with or without leg pain, it is a symptom not a disease.[6] LBP is having multifactorial etiology, major risk factors including, physically demanding work, socioeconomic and employment status, poor general medicine condition, postural factors etc. [7].

Thus, the objectives of present study were to measure Cobb's angle and Ferguson's angle on MRI Images (T2w) in patients with low back pain.

MATERIAL AND METHODS

The present cross-sectional study was carried out in the Department of Anatomy, Radiology, and patients were recruited from the Department of Orthopedics, Physical Medicine and Rehabilitation, Doon Hospital, Government Doon Medical College, Dehradun. The sample size of the study was 210.

All patient's suffering from low back pain above the age of 20 years attending the Department of PMR & Orthopaedics, Doon Hospital, Government Doon Medical College, Dehradun (UK) were included in the study. Patients less than 20 years of age having traumatic low back pain, apparent spinal deformity, history of spinal surgery, hip replacement surgery, knee replacement surgery, Pott's spine, osteoporosis, malignancy, tumour, metastasis, and pregnant females were excluded from the study.

The MRI images of patients were imported into the Autocad 2024 software, and lines were drawn over the cranial endplate of L1 and S1 vertebrae, to measure the Cobb's angle and a line parallel to horizontal was drawn intersecting the line over cranial endplate of S1 vertebra to measure Ferguson's angle. The data thus obtained was analyzed using descriptive statistics, and Pearson correlation by Statistical Package for the Social Sciences (SPSS), version 27.0.

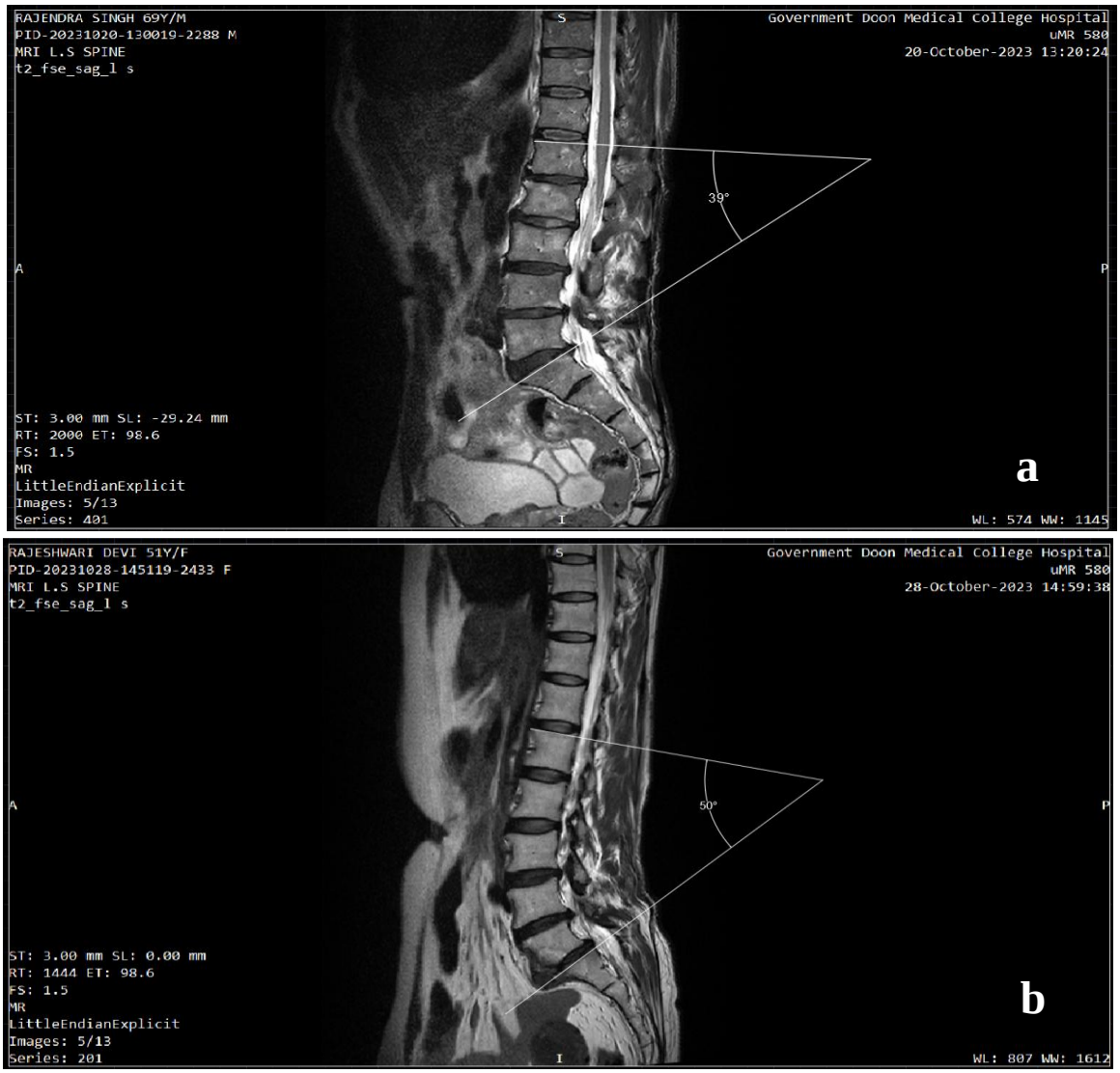

Fig. 1. Showing measurement of Cobb's angle in a female patient.

RESULTS

In the present study, MRI images of total 210 patients were taken for measurement of Cobbs angle and Ferguson's angle on T2 weighted images (5th section) using Autocad software version 2024. (Fig. 1 & Fig. 2)

Of the total samples, the mean Cobb's angle was 44.60° ± 11.390° and the mean Ferguson's angle was 37.63° ± 8.027°. On statistical analysis there was a strong positive correlation (r = 0.925) between the two, and the p- value <0.001 suggested that they are statistically significant. (Table 1)

In males, the mean Cobb's angle was 42.65° ± 10.397° and Ferguson's angle was 37.21° ± 7.461°, again with statistically significant (p-value <0.001), strong positive correlation (r = 0.927). It was also observed that the mean cobb's angle was maximum (49.42° ± 8.764°) in the age group of 50-59 years, and

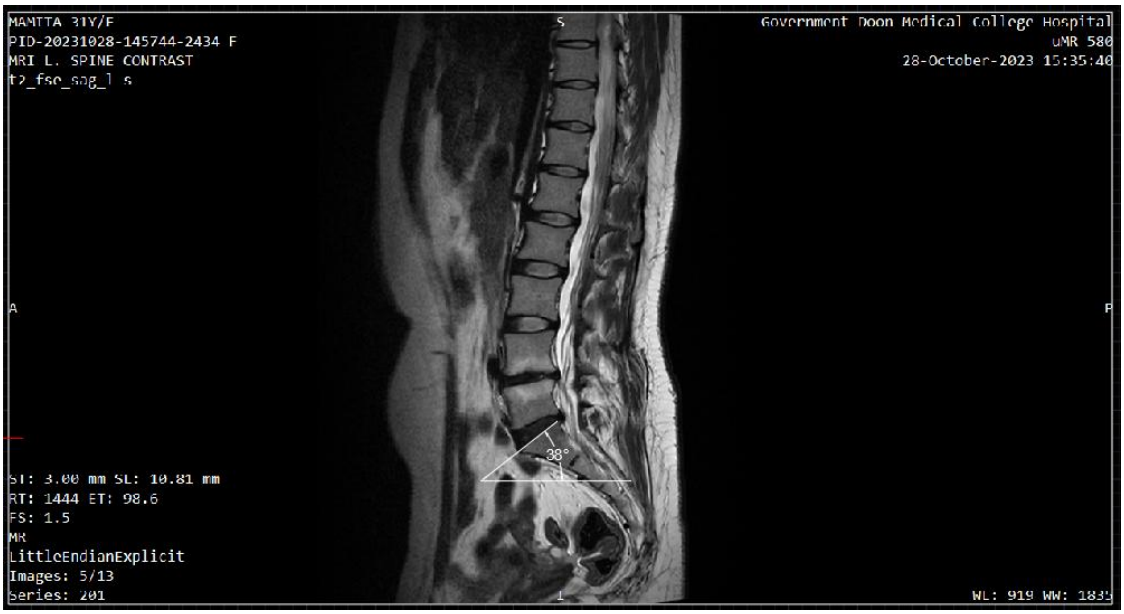

Fig. 2. Ferguson's angle measured digitally on Autocad Software.

Table 1: Showing mean Age and mean Cobb's angle and Ferguson's angle with correlation in males and females

Gender	Mean Age	No. of cases (n)	Mean Cobb's Angle	Mean Ferguson's Angle	r-value
Male	42.30 ± 15.354	92	42.65° ± 10.397°	37.21° ± 7.461°	0.927
Female	43.71 ± 13.548	118	46.11° ± 11.932°	37.97° ± 8.459°	0.931
			p-value = 0.029	p-value = 0.498	

Table 2: Mean Cobb's angle and Ferguson's angle in different age groups with correlation

S. No.	Age Groups	No. of cases (n)	Mean Cobb's Angle	Mean Ferguson's Angle	r-value	p-value
1	20-29	46	42.93° ± 10.008°	36.15° ± 7.366°	0.878	<0.001
2	30-39	41	41.85° ± 9.334°	35.58° ± 6.211	0.906	<0.001
3	40-49	56	43.68° ± 11.808°	37.22° ± 8.164°	0.943	<0.001
4	50-59	31	48.52° ± 11.108°	39.68° ± 7.231	0.942	<0.001
5	60-69	21	46.62° ± 12.882°	40.52° ± 10.323	0.965	<0.001
6	70-79	12	51.17° ± 14.917°	41.08° ± 10.561°	0.897	<0.001

minimum (40.43° ± 9.521°) in the age group of 20-29 years, while Ferguson's angle was maximum (40.75° ± 6.298°) in the age group of 50-59 years, and minimum (35.75° ± 6.602°) in age group of 70-79 years. (Fig 1-a & Table 3)

In females, the mean Cobb's angle was 46.11° ± 11.932° and Ferguson's angle was 37.97° ± 8.459°, again with statistically significant (p-value <0.001), strong positive correlation (r = 0.931). it was also observed that the mean cobb's angle was maximum (55.50° ± 16.283°) in the age group of 70-79 years, and minimum (41.53° ± 6.737°) in the age group of 30-39 years, while Ferguson's angle was maximum (44.50° ± 10.420°) in the age group of 60-69 years, and minimum (34.18° ± 4.626°) in age group of 20-29 years. (Fig 1-b & Table 4)

There was statistically significant difference in the Cobbs angle of both genders, p-value = 0.029, while the Ferguson's angle showed no statistically significant difference, p-value = 0.498. (Table 1)

In all the age groups in both the genders Cobb's angle and Ferguson's angle were statistically and positively correlated. (Table 2) The mean value of Likert pain scale was 6.24 ± 1.544, in males it was 6.36 ± 1.587 while in females it was 6.14 ± 1.509. There was a statistically significant correlation between Likert pain scale and Cobb's angle (p = 0.008) and Ferguson's angle (p = 0.005) in males, while in females only between Likert pain scale and Cobb's angle (p = 0.019). There was no statistically significant correlation between Likert pain scale and Ferguson's angle in females (p = 0.121). The mean Likert pain scale scores tend to increase with age for both males and females, suggesting that older individuals may experience higher levels of pain associated with their spinal conditions. (Table 3 & Table 4)

Table 3: Mean Cobb's angle and Ferguson's angle in different age groups with correlation

S. No.	Age Groups	No. of cases (n)	Mean Cobb's Angle	Mean Ferguson's Angle	r-value	p-value	Mean Likert pain scale
1	20-29	21	40.43° ± 9.521°	36.10° ± 6.833°	0.861	<0.001	5.95 ± 1.396
2	30-39	24	42.08° ± 10.946°	37.04° ± 6.975°	0.968	<0.001	6.38 ± 1.861
3	40-49	18	41.33° ± 10.825°	36.06° ± 7.892°	0.954	<0.001	6.33 ± 1.645
4	50-59	12	49.42° ± 8.764°	40.75° ± 6.298°	0.875	<0.001	6.75 ± 1.485
5	60-69	13	42.92° ± 11.536°	38.08° ± 9.861°	0.956	<0.001	6.15 ± 1.345
6	70-79	4	42.50° ± 6.856°	35.75° ± 6.602°	0.968	0.032	8 ± 0.816

Table 4: Mean Cobb's angle and Ferguson's angle in Females along different age groups with correlation

S. No.	Age Groups	No. of cases (n)	Mean Cobb's Angle	Mean Ferguson's Angle	r-value	p-value	Mean Likert pain scale
1	20-29	25	45.04° ± 10.106°	36.20° ± 7.927°	0.929	<0.001	5.24 ± 1.20
2	30-39	17	41.53° ± 6.737°	34.18° ± 4.626°	0.773	<0.001	6.06 ± 1.638
3	40-49	41	44.71° ± 12.199°	37.73° ± 8.325°	0.940	<0.001	6.39 ± 1.579
4	50-59	19	47.95° ± 12.536°	39° ± 7.853°	0.969	<0.001	6.32 ± 1.376
5	60-69	8	52.63° ± 13.394°	44.50° ± 10.420°	0.975	<0.001	6.75 ± 1.488
6	70-79	8	55.50° ± 16.283°	43.75° ± 11.498°	0.887	0.003	6.88 ± 1.126

DISCUSSION

In the present study there was a statistical positive correlation between the Cobb's angle and the Ferguson's angle (r = 0.925; p <0.001), indicating that as Cobbs angle increases, Ferguson's angle tends to increase too. Both males and females show strong correlations between Cobb's angle and Ferguson's angle across different age groups.

The mean Cobbs angle and mean Ferguson's angle was 44.60° ±11.390° and 37.63° ± 8.027 respectively which was found to be similar with the study of J. Abbas et al [16] where mean Cobbs angle was 42.8° ± 7° and mean Ferguson's angle was 38.5° ± 7°. Mean Cobbs angle in the study done by Jeanie F bailey et al [12] was 46.46 ± 1.74 whereas, mean Ferguson's angle was found to be on higher side 42.57° ± 1.50° when compared to present study.

The greatest mean Cobbs angle reported was observed by Michiel M A Janssen et al [17] 58° ± 10° and mean Ferguson's angle was 41° ± 8.6° followed by Waqas Noor Chugtai et al 57.32° ± 12.45° and 38.10° ± 7.94° respectively [9].

Francis osita okpala et al [13] found highest mean Ferguson's angle 44.17° ± 10° and mean Cobbs angle was observed 49.9 ± 12.8. Izaya Ogon et al [10] and Burbam Faith Kocyigit and Ejder Berk [11] found mean Cobbs angle and mean Ferguson's angle on the lowest side with slight difference in both the angles 5 ± 2.9 &31.1° ± 1.3° and 40.25° ± 9.01° & 40.62° ± 6.85° respectively when compared to others and the present study. (Table 5). This difference is seen due the different ethnicity of the population, population size etc.

Table 5. Comparison of similar studies with the present study.

S. No	Year	Author	Sample size	Mean Cobbs angle	Mean Ferguson's angle
1	2024	Present study	210	44.60° ±11.390°	37.63° ± 8.027
2	2023	Babak Mirzashahi et al[8]	148	54.8° ± 13.7°	35.9° ± 8.6°
3	2023	Waqas Noor Chugtai et al[9]	129	57.32° ± 12.45°	38.10° ± 7.94°
4	2022	Izaya Ogon et al[10]	47	31.5 ± 2.9	31.1° ± 1.3°
5	2018	Burbam Faith Kocyigit and Ejder Berk[11]	202	40.25° ± 9.01°	40.62° ± 6.85°
6	2016	Jeanie F bailey et al[12]	36	46.46 ± 1.74	42.57° ± 1.50°
7	2014	Francis osita okpala et al[13]	200	49.9 ± 12.8	44.17° ± 10°
8	2014	Zhu et al[14]	260	48.2 ± 9.6	32.5° ± 6.5°
9	2011	Chung Suh Lee et al[15]	86	49.6° ± 9.6°	36.3° ± 7.8°
10	2010	J Abbas et al[16]	67	42.8° ± 7°	38.5° ± 7°
11	2009	Michiel M A Janssen et al [17]	60	58° ± 10°	41° ± 8.6°

CONCLUSION

This study concluded that with increasing pain both the Cobb's and Ferguson's angles increase. Both, Cobb's angle and Ferguson's angle also tend to increase with advancing age. The Cobb's angle was found to be on higher side in females. Measurement of Cobb's and Ferguson's angle gives us a direct idea of spinal curvature thus assessing the severity of the condition (low back pain) These angles will be helpful in targeted assessment and interventional strategies, creating personalized treatment plans and formulating proper rehabilitation protocol like specific individualized strengthening exercises of spinal muscles, appropriate nutritional supports, maintenance of proper posture, and ergonomics alongside workplace modifications to prevent abnormal lumbar curvatures.

Limitations: The limitations of this study is that the number of subjects in each age group are not same.

REFERENCES

1. Standring S, Gray H. Gray's anatomy: the anatomical basis of clinical practice [Internet]. 41st ed. Elsevier; 2020 [cited 2025 May 29].
2. Jha AK, Ravi C. A study of normal variation in lumbosacral angle in asymptomatic patients attending orthopaedic out-patient department of a medical college hospital, Telangana. Indian J Orthop Surg. 2018;4(1):16–20.
3. Sparrey CJ, Bailey JF, Safaee M, Clark AJ, Lafage V, Schwab F, et al. Etiology of lumbar lordosis and its pathophysiology: a review of the evolution of lumbar lordosis, and the mechanics and biology of lumbar degeneration. Neurosurg Focus. 2014;36(5):E1.
4. Habibi Z, Maleki F, Meybodi AT, Mahdavi A, Saberi H. Lumbosacral sagittal alignment in association to intervertebral disc diseases. Asian Spine J [Internet]. 2014 Dec;8(6):813–9.
5. Tüzün Ç, Yorulmaz İ, Cindaş A, Vatan S. Low back pain and posture. Clin Rheumatol [Internet]. 1999 Jun 1;18(4):308–12.
6. De Vet HCW, Heymans MW, Dunn KM, Pope DP, van der Beek AJ, Macfarlane GJ, et al. Episodes of low back pain: a proposal for uniform definitions to be used in research. Spine (Phila Pa 1976). 2002;27(21):2409–16.
7. Chaléat-Valayer E, Mac-Thiong JM, Paquet J, Berthonnaud E, Siani F, Roussouly P. Sagittal spino-pelvic alignment in chronic low back pain. Eur Spine J [Internet]. 2011 Sep 26;20(S5):634–40.
8. Mirzashahi B, Hajializade M, Kordkandi SA, Farahini H, Moghtadaei M, Yeganeh A, et al. Spinopelvic parameters as risk factors of nonspecific low back pain: a case-control study. Med J Islam Repub Iran. 2023;37(1):1–7.
9. Chughtai WN, Fatima T, Rashid A, Razzaque MA, Ullah MA. Significance of correlation between spinopelvic parameters in patients of chronic low back pain. Pak J Neurol Surg. 2023;27(2):259–68.
10. Ogon I, Teramoto A, Takashima H, Terashima Y, Yoshimoto M, Emori M, et al. Factors associated with low back pain in patients with lumbar spinal stenosis: a cross-sectional study. BMC Musculoskelet Disord. 2022;23(1):388.
11. Kocyigit BF, Berk E. Comparison of lumbosacral alignment in geriatric and non-geriatric patients suffering low back pain. Pak J Med Sci. 2018;34(2):291–5.
12. Bailey JF, Sparrey CJ, Been E, Kramer PA. Morphological and postural sexual dimorphism of the lumbar spine facilitates greater lordosis in females. J Anat. 2016;229(1):82–91.
13. Okpala F. Measurement of lumbosacral angle in normal radiographs: a retrospective study in Southeast Nigeria. Ann Med Health Sci Res.

2014;4(5):757–60.

14. Zhu Z, Xu L, Zhu F, Jiang L, Wang Z, Liu Z, et al. Sagittal alignment of spine and pelvis in asymptomatic adults: norms in Chinese populations. Spine (Phila Pa 1976). 2014;39(1):E1–6.
15. 15. Lee CS, Chung SS, Kang KC, Park SJ, Shin SK. Normal patterns of sagittal alignment of the spine in young adults: radiological analysis in a Korean population. Spine (Phila Pa 1976). 2011;36(25):E1648–54.
16. 16. Abbas J, Hamoud K, May H, Hay O, Medlej B, Masharawi Y, et al. Degenerative lumbar spinal stenosis and lumbar spine configuration. Eur Spine J. 2010;19(11):1865–73.
17. 17. Janssen MMA, Drevelle X, Humbert L, Skalli W, Castelein RM, Veldhuizen AG. Differences in male and female spino-pelvic alignment in asymptomatic young adults: a three-dimensional analysis using upright low-dose digital biplanar X-rays. Spine (Phila Pa 1976). 2009;34(23):E826–32.

https://doi.org/10.46351/jas.v32i2pp88-98

JAS Journal of Anatomical Sciences (U.P. Chapter of Anatomical Society of India)

Original Article

Cholelithiasis-associated gallbladder mucosal alterations: A histopathological analysis with clinical correlation

Mudassar Imam[1], Satyam Khare[1], Shilpi Jain[1], Ram Kumar Kaushik[1], Pooja Dawani[1]

1. Department of Anatomy, Subharti Medical College, Meerut, India

ABSTRACT

Introduction: Cholelithiasis is a common condition with significant histopathological consequences for the gallbladder mucosa, ranging from chronic inflammation to potential malignant transformation. This study aimed to assess the spectrum of microscopic changes in gallbladder specimens from cholelithiasis patients and their correlation with clinical parameters.

Materials and Methods: A cross-sectional, observational study was conducted over two years at the Department of Pathology, Subharti Medical College, Meerut. A total of 100 cholecystectomy specimens from adult patients diagnosed with cholelithiasis were examined. Routine histopathological procedures were employed, and sections were stained with Hematoxylin and Eosin. Additional stains were used when necessary. Findings were correlated with demographic and clinical data, and statistical analysis was performed using SPSS v25.0.

Results: The majority of patients were female (68%), with the highest prevalence in the 41–50 age group. Chronic cholecystitis was observed in 90% of cases, Rokitansky-Aschoff sinuses in 40%, epithelial hyperplasia in 10%, fibrosis/ulceration in 5%, and carcinoma in 2%. Statistically significant associations were found between age and the presence of Rokitansky-Aschoff sinuses ($p<0.05$). Carcinoma cases occurred exclusively in female patients above 50 years of age.

Conclusions: Chronic inflammatory changes are predominant in gallbladders affected by cholelithiasis. The presence of epithelial hyperplasia and incidental carcinoma emphasizes the necessity for routine histopathological examination of all cholecystectomy specimens to detect early neoplastic changes, particularly in high-risk populations.

Keywords: Cholelithiasis, Gallbladder, Chronic Cholecystitis, Rokitansky-Aschoff Sinuses, Epithelial Hyperplasia, Gallbladder Carcinoma, Histopathology

Address for Correspondence:
Dr. Satyam Khare, Professor & Head, Department of Anatomy, Subharti Medical College, Meerut, India
Email: dr_kharesatyam@yahoo.com Mob.: 9837083748

Date of Receiving: 27 Sep 2024
Date of Acceptance: 03 Nov 2024

INTRODUCTION

Located beneath the liver, the gallbladder is a small, pear-shaped organ responsible for storing and concentrating bile. Anatomically, it is composed of serosal, muscular, and mucosal layers, with the mucosa lined by simple columnar epithelium. Its strategic location and function make it susceptible to a variety of pathological conditions, one of the most common being cholelithiasis, or gallstone disease. Gallstones form primarily due to the precipitation of cholesterol, bile pigments, and calcium salts, and can lead to significant clinical complications, including acute and chronic cholecystitis, mucosal hyperplasia, and even malignancy [1].

Cholelithiasis is a prevalent condition worldwide, with variable prevalence rates depending on geographic, dietary, and genetic factors [2]. In India, the prevalence ranges from 2% to 29%, with higher rates observed in certain Northern states due to specific lifestyle and dietary patterns [3]. The pathogenesis of gallstones is multifactorial, involving alterations in bile composition, gallbladder motility, and the presence of nucleating factors that initiate the crystallization process [4]. Gallstones, especially when asymptomatic, can remain undetected for years; however, when symptomatic, they are often associated with right upper quadrant abdominal pain, nausea, and other gastrointestinal symptoms [5].

Histopathological examination of the gallbladder in patients undergoing cholecystectomy for cholelithiasis has revealed a spectrum of changes, ranging from chronic inflammation (chronic cholecystitis) to more severe alterations, such as Rokitansky-Aschoff sinuses, epithelial hyperplasia, metaplasia, and in rare cases, dysplasia or carcinoma [6]. Chronic irritation caused by the presence of gallstones is a significant factor leading to these changes, as it triggers a cycle of epithelial injury, inflammation, and repair, which over time may contribute to malignant transformation [7].

Chronic cholecystitis, marked by ongoing inflammation of the gallbladder wall, is the most commonly observed histopathological change in gallbladder specimens linked to cholelithiasis. Histologically, It typically shows accumulation of lymphocytes, plasma cells, and sometimes eosinophils into the lamina propria [8]. Rokitansky-Aschoff sinuses, another common feature, are mucosal invaginations extending into the muscular layer, often considered a response to chronic inflammation and increased intraluminal pressure [9]. Epithelial hyperplasia, which may range from simple to adenomatous patterns, is also observed and poses a risk for malignant transformation in a subset of cases [10].

Recent research has emphasized a link between prolonged gallbladder inflammation

and the onset of gallbladder cancer, particularly in areas where cholelithiasis is highly prevalent. Gallbladder cancer continues to be among the most aggressive types of malignancies affecting the biliary tract, with poor prognosis due to its late presentation [4]. Therefore, routine histopathological examination of all cholecystectomy specimens, even in cases of clinically benign disease, is essential for early detection of pre-malignant and malignant changes [2].

This study aimed to examine the microscopic pathological alterations in the gallbladder lining associated with cholelithiasis, to better understand the spectrum of alterations, and to emphasize the importance of routine histological examination in patients undergoing cholecystectomy. By correlating the presence of histopathological changes with clinical parameters, this study seeks to contribute to the understanding of the pathophysiology of cholelithiasis and its complications, providing insights into potential preventive and therapeutic strategies.

MATERIAL AND METHODS

Study Design and Setting: A cross-sectional, observational study was carried out in the Department of Pathology at Subharti Medical College, Meerut, spanning two years from January 2022 to December 2023. During this period, 100 gallbladder specimens were obtained from patients diagnosed with cholelithiasis who had undergone cholecystectomy which were confirmed via clinical, radiological, and surgical findings. Ethical clearance for the study was granted by the institutional ethics committee, and informed consent was secured from all participants.

Inclusion Criteria:

- Individuals undergoing planned or urgent cholecystectomy with a verified diagnosis of cholelithiasis.
- Both symptomatic and asymptomatic cases were included.
- Specimens from adult patients (age ≥ 18 years) of both genders.

Exclusion Criteria:

- Specimens with a history of primary gallbladder malignancy detected pre-operatively.
- Patients with known chronic liver disease or other biliary tract disorders.
- Specimens showing autolytic changes or improper fixation.

The cholecystectomy specimens were collected immediately after surgery, labeled, and transferred to the pathology department. Each specimen was thoroughly inspected for external and internal features, including the presence of stones, wall thickness, mucosal appearance, and any gross abnormalities. After recording the gross findings, to maintain tissue integrity, the specimens were preserved in 10% neutral buffered formalin for 24 to 48 hours.

Following fixation, the specimens were processed using standard histopathological techniques:

1. Tissue Sampling: Tissue samples were selectively obtained from the fundus, body, and neck regions of the gallbladder, along with any visible abnormal areas, such as polyps, nodules, or areas of thickening.
2. Dehydration and Embedding: The tissues underwent dehydration through increasing concentrations of ethanol, were then cleared using xylene, and finally embedded in paraffin wax blocks.
3. Section Cutting and Staining: Slices measuring 4-5 µm in thickness were prepared with a microtome and stained with Hematoxylin and Eosin (H&E) for microscopic analysis. When needed, extra stains such as Periodic Acid-Schiff and Alcian Blue were applied to highlight particular histopathological characteristics.

Histopathological Examination

The prepared slides were examined under a light microscope by two independent pathologists to ensure accuracy. The histopathological changes observed were categorized into the following:

1. Chronic Cholecystitis: Defined by lymphoplasmacytic infiltration, fibrosis, and the presence of lymphoid aggregates.
2. Rokitansky-Aschoff Sinuses (RAS): Identified as invaginations of the mucosa extending into the muscular layer.
3. Epithelial Hyperplasia: Including both simple and adenomatous hyperplasia, characterized by the thickening of the mucosal epithelium.
4. Fibrosis and Ulceration: Presence of fibroblastic proliferation and loss of mucosal continuity, respectively.
5. Dysplasia and Carcinoma: Cases exhibiting cellular atypia, pleomorphism, and mitotic figures were subjected to further immunohistochemical analysis to confirm malignant transformation.

Each histopathological finding was documented, and the frequency of different types of changes was recorded. The presence of specific patterns was noted, and their correlation with clinical parameters (e.g., age, gender, duration of symptoms) was analyzed.

Statistical Analysis

The data were recorded in a Microsoft Excel spreadsheet and analyzed using SPSS software version 25.0. Descriptive statistics were employed to determine the frequency and percentage of the histopathological findings. For continuous variables, the mean and standard deviation (SD) were calculated, whereas categorical variables were presented as percentages. Chi-square tests were used to evaluate the relationship between clinical factors (including age and gender) and particular histopathological findings. A p-value less than 0.05 was regarded as statistically significant.

This study was carried out following the principles of the Declaration of Helsinki. Prior to starting, approval was secured from the Institutional Ethics Committee of Subharti Medical College, Meerut. To ensure confidentiality, all patient information was anonymized, and no personal identifiers were included in the final analysis.

RESULTS

Demographic Profile

A total of 100 cholecystectomy specimens from patients diagnosed with cholelithiasis were analyzed. The patients' ages varied between 18 and 75 years, with an average age of 45.6 ± 12.4 years. The age group with the highest occurrence was 41-50 years, accounting for 32% of cases. The study population consisted of 68 females (68%) and 32 males (32%), resulting in a female-to-male ratio of 2.1:1, indicating a higher prevalence of cholelithiasis in females.

Clinical Presentation

The most common clinical presentation was chronic upper abdominal pain, reported in 78% of the patients. Other symptoms included nausea (42%), vomiting (30%), and jaundice (8%). Asymptomatic cases were detected in 12% of the patients during routine health evaluations.

Gross Pathological Findings

On gross examination, all gallbladder specimens had gallstones, with 84% showing multiple stones and 16% showing a single large stone. The stones ranged in diameter from 0.5 cm to 3.5 cm. Thickening of the gallbladder wall (>3 mm) was observed in 68% of the cases, while

Table 1. Demographic Distribution of Patients.

Age Group (Years)	Male	Female	Total (%)
18-30	5	8	13 (13%)
31-40	7	15	22 (22%)
41-50	10	22	32 (32%)
51-60	5	14	19 (19%)
>60	5	9	14 (14%)
Total	32	68	**100 (100%)**

Table 2. Gross Pathological Features.

Feature	Frequency (%)
Multiple Stones	84
Single Stone	16
Thickened Gallbladder Wall	68
Mucosal Erythema/Irregularity	52

mucosal erythema and irregularity were noted in 52% of the specimens.

Histopathological Findings

The histopathological examination of the 100 gallbladder specimens revealed a variety of changes associated with cholelithiasis. (Fig. 1) Chronic cholecystitis was the predominant finding, present in 90% of cases, followed by Rokitansky-Aschoff sinuses (RAS) in 40% (Fig. 1(b)), epithelial hyperplasia in 10% (Fig. 1(c)), and fibrosis or ulceration in 5% (Fig. 1(d)). Carcinoma was detected in 2% of the specimens (Fig. 1(e & f)).

Correlation of Histopathological Findings with Clinical Parameters

Age and Histopathological Changes:

• Chronic cholecystitis was observed in all age groups, showing a slightly higher occurrence in patients between 41 and 60 years of age.

• Rokitansky-Aschoff sinuses were more commonly observed in older age groups (>50 years), suggesting a prolonged history of gallstone disease.

• Epithelial hyperplasia and carcinoma were observed primarily in patients above 50 years of age.

Gender and Histopathological Changes:

Both males and females showed similar patterns of chronic cholecystitis and Rokitansky-Aschoff sinuses. However, carcinoma was detected only in female patients.

Statistical Analysis: Chi-square analysis revealed a statistically significant correlation between age and the presence of

Table 3. Histopathological findings in Gallbladder specimens.

Histopathological Finding	Number of Cases	Frequency (%)
Chronic Cholecystitis	90	90%
Rokitansky-Aschoff Sinuses	40	40%
Epithelial Hyperplasia	10	10%
Fibrosis and Ulceration	5	5%
Carcinoma	2	2%

Table 4. Association Between Age and Histopathological Findings.

Age Group (Years)	Chronic Cholecystitis	RAS	Epithelial Hyperplasia	Carcinoma
18-30	12	4	0	0
31-40	21	8	2	0
41-50	30	14	4	0
51-60	17	10	3	1
>60	10	4	1	1

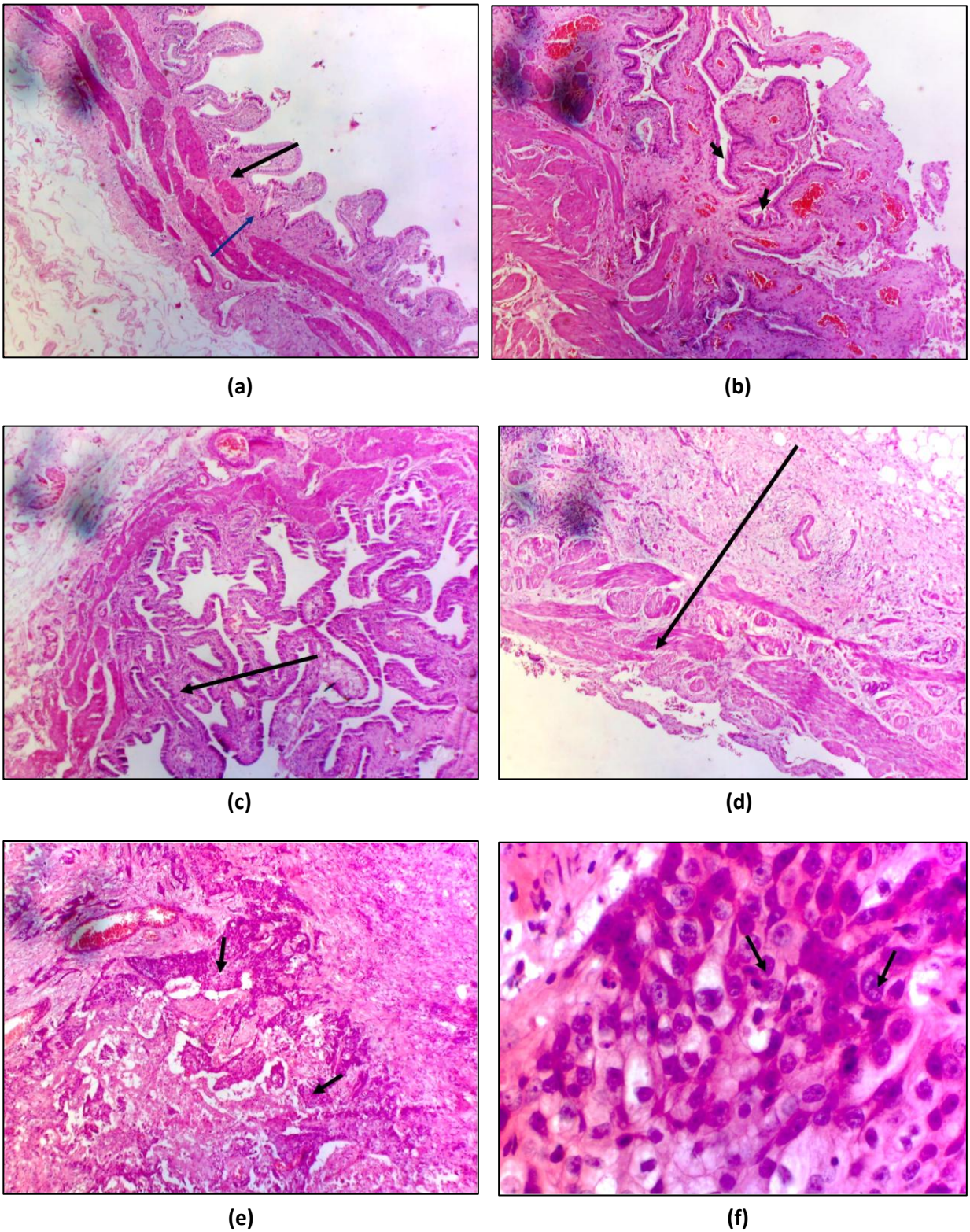

Fig. 1. Transverse section (10x) of human Gall bladder. (a) Normal; black arrow – mucosal layer; blue arrow – fibromuscular layer (b) Chronic cholecystitis with Rokitansky Aschoff sinuses (arrows) (c) Epithelial hyperplasia (d) Transmural fibrosis (e) Carcinoma (10x) (f) Carcinoma (40x)

Rokitansky-Aschoff sinuses ($p<0.05$), indicating a higher likelihood of RAS formation in older patients. The association between gender and carcinoma, though limited by the small number of cases, was also noted ($p<0.05$).

Summary of Key Findings

1. Chronic Cholecystitis was the predominant histopathological alteration, found in 90% of the cases, underscoring the chronic inflammatory process associated with gallstone disease.
2. Rokitansky-Aschoff Sinuses were seen in 40% of the specimens, suggesting long-standing irritation of the gallbladder wall.
3. Epithelial Hyperplasia was identified in 10% of cases, which could represent early precancerous changes.
4. Carcinoma was found in 2% of the specimens, highlighting the importance of routine histopathological examination for early detection of malignancy.

These findings indicate a strong association between gallstones and various histopathological alterations in the gallbladder mucosa, highlighting the importance of thorough examination of all cholecystectomy specimens to detect or exclude early malignant changes.

DISCUSSION

Cholelithiasis, or gallstone disease, remains a significant health concern worldwide, particularly in regions where dietary habits, genetic predisposition, and other risk factors contribute to its high prevalence. The purpose of this study was to examine the histopathological alterations in the gallbladder mucosa linked to cholelithiasis and to understand their correlation with clinical parameters. Our findings are consistent with existing literature, which underscores the variety of histopathological alterations that can occur due to the chronic inflammatory effects of gallstones.

The most frequent histopathological change observed In this study was chronic cholecystitis which was observed in 90% of the cases. This aligns with previous reports indicating that chronic inflammation is the hallmark of gallstone disease, often resulting from prolonged mucosal irritation caused by the physical presence of stones [4,10].

Table 5: Comparison of Histopathological Findings with Previous Studies

Study	Chronic Cholecystitis (%)	RAS (%)	Hyperplasia (%)	Carcinoma (%)
Present Study	90	40	10	2
Zahrani & Mansoor[9]	97	33.2	8	1.5
Mohan et al.[20]	88	38	12	3

Chronic cholecystitis is marked by the presence of lymphocyte and plasma cell infiltration, with varying degrees of fibrosis, which were also observed in our samples [11]. Studies suggest that persistent irritation can lead to a cycle of epithelial damage and repair, predisposing the mucosa to further alterations, such as hyperplasia and metaplasia [12].

Rokitansky-Aschoff sinuses were identified in 40% of the samples. These mucosal outpouchings are considered pseudodiverticula that form as a response to chronic inflammation and increased intraluminal pressure [6,13]. The formation of RAS is often associated with longstanding gallstone disease, and their presence was more common in older patients in our study, indicating a possible correlation with the duration of the disease process. Similar findings have been reported in previous studies, where the prevalence of RAS ranged between 30% and 45% among patients with cholelithiasis [14].

Epithelial hyperplasia was noted in 10% of the specimens, raising concerns about the risk of progression to dysplasia and malignancy. Hyperplasia, marked by a rise in the quantity of epithelial cells, can be an adaptive response to chronic irritation but may also serve as a precursor to neoplastic changes [15]. The transition from hyperplasia to dysplasia and eventually carcinoma has been documented in the literature, suggesting a continuum of mucosal changes driven by chronic inflammation and cellular stress [16]. In regions with high gallstone prevalence, the incidence of gallbladder cancer has also been noted to be higher, emphasizing the need for vigilance in monitoring histopathological changes in cholecystectomy specimens [2].

The identification of carcinoma in 2% of the specimens underscores the importance of routine histopathological examination of all cholecystectomy specimens, even in the absence of pre-operative suspicion of malignancy. Gallbladder cancer is an uncommon yet highly aggressive tumor with a poor prognosis, frequently diagnosed at a late stage because of its vague symptoms and delayed clinical presentation [5,17]. Our findings underscore the need for early detection of malignancy, which can be facilitated by identifying precursor lesions including dysplasia and carcinoma in situ detected during routine examination [18]. The relationship between gallstone disease and gallbladder cancer has been well-documented, particularly in nations where gallstones are highly prevalent, such as India and Chile [6,7].

Our study found a higher prevalence of gallstone disease and associated histopathological alterations more commonly in females, showing a female-to-male ratio of 2.1:1, which aligns with worldwide data, which

suggests that hormonal factors, particularly estrogen, may play a role in gallstone formation and subsequent mucosal changes [5,19]. The increased risk among females may also be related to pregnancy, use of oral contraceptives, and obesity, all of which are known risk factors for gallstone disease [8,20]. Awareness of these gender-specific risk factors is crucial for early diagnosis and management.

The spectrum of histopathological changes observed in our study is in line with those reported by other researchers. Zahrani and Mansoor reported a similar distribution, with chronic cholecystitis being the predominant finding in their study, followed by RAS and hyperplasia [9]. Another study from North India highlighted a comparable prevalence of epithelial hyperplasia and carcinoma, particularly in older patients, suggesting a link between age and the risk of malignant transformation [20]. However, variations in the incidence of certain lesions, such as carcinoma, may be attributed to differences in sample size, geographic location, and patient demographics.

The primary limitation of this study was its relatively small sample size, which could restrict the applicability of the results. Furthermore, the research was carried out at a single institution, and thus, regional variations in the incidence of histopathological changes may not be fully represented. Further, more extensive multi-center research with greater sample sizes is required to confirm these results and to examine the molecular processes driving the progression from benign to malignant changes.

CONCLUSION

This study highlights the spectrum of histopathological changes associated with cholelithiasis, with chronic cholecystitis being the most common finding. The identification of precursor lesions like epithelial hyperplasia highlights the crucial role of routine histopathological analysis of cholecystectomy specimens in detecting early neoplastic alterations. The correlation between gallstone disease and gallbladder carcinoma emphasizes the need for preventive strategies and heightened clinical awareness, particularly in high-risk populations.

REFERENCES

1. Ransohoff DF, Gracie WA. Treatment of gallstones. Ann Intern Med. 1993;119(7 Pt 1):606-619.
2. Shaffer EA. Gallstone disease: Epidemiology of gallbladder stone disease. Best Pract Res Clin Gastroenterol. 2006;20(6):981-996.
3. Schirmer BD, Winters KL, Edlich RF. Cholelithiasis and cholecystitis. J Long Term Eff Med Implants. 2005;15(3):329-338.
4. Lammert F, Sauerbruch T. Mechanisms of disease: the genetic epidemiology of

gallbladder stones. Nat Clin Pract Gastroenterol Hepatol. 2005;2(9):423-433.

5. Crawford JM. The liver and the biliary tract. In: Robbins and Cotran Pathologic Basis of Disease. 9th ed. Elsevier; 2015.
6. Stinton LM, Shaffer EA. Epidemiology of gallbladder disease: cholelithiasis and cancer. Gut Liver. 2012;6(2):172-187.
7. Mohan H, Punia RP, Dhawan SB, Ahal S, Sekhon MS. Morphological spectrum of gallstone disease in 1100 cholecystectomies in North India. Indian J Surg. 2005;67(3):140-142.
8. Shukla VK, Singh H, Pandey M, Upadhyay SK, Nath G. Carcinoma of the gallbladder—is it a sequel of gallstone disease? J Surg Oncol. 2006;93(8):607-612.
9. Zahrani IH, Mansoor I. Gallbladder pathologies and cholelithiasis. Saudi Med J. 2001;22(10):885-889.
10. Zuhair M, Mumtaz R. Histological changes of gall bladder mucosa: Correlation with various types of cholelithiasis. Iraqi J Comm Med. 2011;24(3):234-240.
11. Albores-Saavedra J, Henson DE, Klimstra DS. Tumors of the gallbladder, extrahepatic bile ducts, and ampulla of Vater. AFIP Atlas of Tumor Pathology; 2000.
12. Zhang J, Wu G, Wei J. Pathogenesis and clinical significance of Rokitansky-Aschoff sinuses in the gallbladder. Pathol Res Pract. 2010;206(9):622-627.
13. Luna A, Lapsia S, Ahuja N. Gallbladder Pathology in Chronic Cholecystitis. Int J Res Med Sci. 2016;4(5):1537-1540.
14. Bosch FX, Ribes J, Cleries R, Diaz M. Epidemiology of gallbladder cancer. Hepatogastroenterology. 2004;51(55):2003-2008.
15. Chaube A, Sarin R, Jain S. Correlation between epithelial hyperplasia and gallbladder cancer. Indian J Cancer. 2008;45(4):144-148.
16. Hundal R, Shaffer EA. Gallbladder cancer: Epidemiology and outcome. Clin Epidemiol. 2014;6:99-109.
17. Misra S, Chaturvedi A, Misra NC, Sharma ID. Carcinoma of the gallbladder. Lancet Oncol. 2003;4(3):167-176.
18. Hundal R, Wilkinson J. Pathogenesis of gallbladder carcinoma: Chronic inflammation and beyond. J Clin Oncol. 2020;38(10):1131-1137.
19. Paumgartner G. Gallstones: Pathogenesis. The Lancet. 2006;368(9531):1408-1411.
20. Mohan H, Punia RP, Ahal S, et al. Epithelial hyperplasia in cholelithiasis: A risk factor for carcinoma? Indian J Gastroenterol. 2007;26(1):35-38.

https://doi.org/10.46351/jas.v32i2pp99-111

JAS Journal of Anatomical Sciences (U.P. Chapter of Anatomical Society of India)

Original Article

A rare variation of thyroid gland - Isthmus agenesis

Navodita Chaudhary[1]

1. Department of Anatomy, Rajshree Medical College and Research Centre, Bareilly, India

ABSTRACT

Introduction: The thyroid gland, the first endocrine gland to develop embryologically by the third week of gestation, plays a critical role in regulating basal metabolic rate, somatic and psychic growth, and calcium metabolism. Developmental and anatomical abnormalities of the thyroid, particularly agenesis of the isthmus, though rare, can present clinical and surgical challenges. The present study was undertaken to observe and document the morphological variations, particularly isthmus agenesis, in human fetal thyroid glands.

Materials and Methods: The study was conducted on 52 stillborn fetuses (25 male and 27 female), ranging from 10 to 40 weeks of gestation, collected with ethical clearance and appropriate obstetric records. The fetuses were embalmed using 10% formalin by the multiple injection method and systematically dissected. Morphological features of the thyroid gland were examined and recorded, including anomalies such as isthmus agenesis and the presence of levator glandulae thyroidae.

Results: Isthmus agenesis was observed in 2 out of 52 fetuses (3.84%), occurring equally in both sexes (1.92%). In one case, the levator glandulae thyroidae was noted arising from the right lobe. These findings align with previous studies, where the incidence varied from 2% to 33%. No other anomalies or lobar agenesis were found. Thyroid weights and morphometric parameters were consistent with gestational age.

Conclusions: Thyroid isthmus agenesis is a rare, often asymptomatic congenital anomaly. However, unawareness of such variations may complicate surgical procedures or be misinterpreted during imaging. Early recognition is essential for safe surgical planning and accurate diagnosis.

Keywords: Thyroid gland, Isthmus agenesis, Fetal morphology, Levator glandulae thyroidae, Anatomical variation

Address for Correspondence:
Dr. Navodita Chaudhary, Associate Professor, Department of Anatomy, Rajshree Medical College and Research Centre, Bareilly, India
Email: navodita2112@gmail.com Mob.: 8077864374

Date of Receiving: 20 Oct 2024
Date of Acceptance: 02 Dec 2024

INTRODUCTION

The thyroid gland is a key component of the endocrine system, playing a central role in metabolic regulation, growth, and development. Morphologically, it is characterized by a bilobed structure joined by a central isthmus, forming an 'H'-shaped configuration on the anterior aspect of the trachea. Embryologically, the thyroid originates as an endodermal diverticulum from the primitive pharynx and descends to its final cervical location by the seventh gestational week, guided by molecular signaling pathways, including fibroblast growth factor (FGF) and transcription factors such as TITF1, PAX8, and FOXE1 [1–3].

Developmental anomalies of the thyroid gland are not uncommon and may range from agenesis, ectopic thyroid, hemiagenesis, to isthmus agenesis. Among these, isthmus agenesis is a rare variation, with reported incidences ranging from 2% to 33%, depending on population studied, sample size, and methodology [4–8]. While the absence of the isthmus typically has no significant impact on thyroid hormone function, it may complicate surgical procedures or be misinterpreted in radiological imaging as thyroid pathology, such as nodules or neoplasms [9].

The isthmus develops from the thyroglossal duct's midline fusion and failure of this fusion is thought to be the primary cause of its agenesis [10]. Genetic mutations, especially in the PAX8 and TITF1 genes, have been implicated in thyroid developmental disorders, including isolated isthmus agenesis [3,11]. In addition, environmental and epigenetic factors may influence embryonic thyroid morphogenesis, although these remain less clearly understood.

Numerous cadaveric and fetal studies have investigated the morphometry and anomalies of the thyroid gland. Ranade et al. observed a striking 33% absence of the isthmus in their study population [6]. On the other hand, Harjeet et al. reported a more conservative figure of 7.9%, while Pastor Vázquez et al. suggested a range of 5–10% [7,8]. The discrepancy in these values emphasizes the importance of demographic and methodological diversity in anatomical studies. Recognizing such rare anomalies is crucial for surgeons, radiologists, and anatomists alike. During thyroidectomy or other neck surgeries, unawareness of these variants could result in inadvertent complications or misdiagnoses. Furthermore, variations such as levator glandulae thyroidae or pyramidal lobes may coexist with isthmus agenesis, contributing to an even more complex anatomical landscape [12].

The present study was undertaken to investigate the presence and incidence of thyroid isthmus agenesis in stillborn fetuses. Identifying such developmental variations early on may provide insights into congenital

thyroid anomalies and assist clinicians in planning safer and more accurate surgical interventions.

MATERIAL AND METHODS

In the current study, 52 stillborn fetuses (25 males and 27 females) ranging from 10 to 40 weeks of gestation were collected from a maternity hospital, along with corresponding obstetric records from the department. The sample population comprised spontaneously aborted and stillborn fetuses Fetus selection was performed in order to eliminate the ones with obvious developmental anomalies. After procurement of fetuses with due regards on ethical grounds, fetuses were collected in plastic container having 10% formalin solution. The fetuses were weighed on digital weighing machine and then embalmed with 10% formalin solution by multiple injection method (Ajmani method) [13]. Using a 10 ml syringe and 20 number needles, 10% formalin was locally injected into the cranial cavity, thoracic cavity, neck, and subcutaneously in the upper and lower limbs to ensure the fixation of the fetuses.

Gestational age was noted from hospital records. It was calculated from the first day of last menstrual period mentioned in the patient profile. The gross parameters of all fetuses including Crown-rump length (CRL), foot length (FL)of both feet, ear pinna length (EL) of both ears were recorded manually with the help of digital vernier caliper and scale.

After 24 hours of embalming, fetal neck dissections were performed by putting a mid-line incision over the skin of neck region, from the chin to the sternum. The upper end of the incision was extended along the lower border of mandible for 5 cm on each side. The lower end of the incision was extended upwards along the anterior border of the sternocleido-mastoid muscle by 5 cm. and reflecting the skin laterally. After removal of layers of neck, thyroid gland was observed for gross congenital anomalies. Various parameters were recorded manually. Thyroid gland was weighed via digital weighing machine.

The instruments used for dissection and measurement included a digital vernier caliper, a dissecting set comprising scissors, a scalpel with surgical blade, and forceps, along with a standard measuring scale, a digital weighing machine, and a dissecting tray. All data collected during the study were systematically tabulated and subjected to statistical analysis.

RESULTS

A total of 52 human fetuses were included in the present study, consisting of 25 males and 27 females, with gestational ages ranging from 10 to 40 weeks. After careful dissection and examination, isthmus agenesis of the thyroid gland was observed in 2 fetuses, yielding an overall incidence of 3.84%. This anomaly was present in one male (Fig. 1(a)) and one female fetus (Fig. 1(b)), contributing

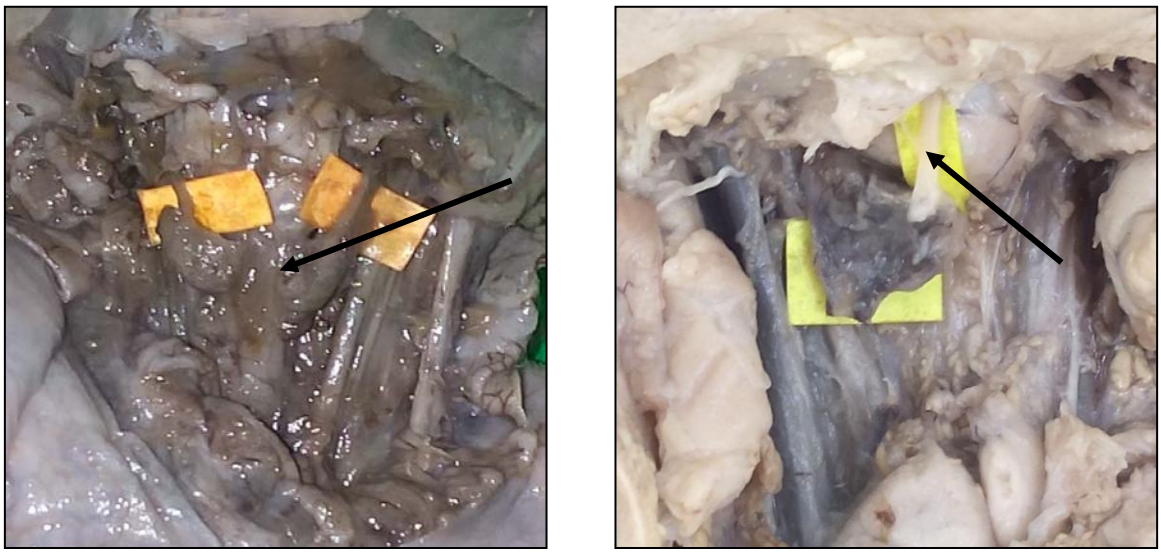

(a) (b)

Fig. 1. (a) Right and left lobes and isthmus agenesis of thyroid gland in a male fetus of 18 weeks of gestation (arrow indicates absence of isthmus of thyroid gland); (b) left lobe and isthmus agenesis, levator glandulae thyroidae attached to right lobe of thyroid gland in situ in a female fetus of 27 weeks of gestation (arrow indicates , levator glandulae thyroidae attached to right lobe of thyroid gland).

equally (1.92%) to the incidence. In one female fetus aged 27 weeks, the levator glandulae thyroidae was found arising from the right lobe of the thyroid gland and extending toward the hyoid bone, in the absence of the isthmus.

The thyroid lobes were located in their typical anatomical positions on either side of the trachea, even in cases where the isthmus was absent. Morphometric assessment of the thyroid lobes—including length, breadth, and thickness—was performed manually using a digital vernier caliper (Table 1). The glands were found to be well-formed, and the size of the lobes was proportional to gestational age, without any gross asymmetry. Though isthmus agenesis was the only anomaly encountered in this study, morphometric variations between the two affected fetuses were evident. The thyroid weights of these fetuses were lower than the group mean, though still within expected ranges for their gestational ages. In the fetus with levator glandulae thyroidae, the structure was distinctly visible and measured during dissection.

No other congenital malformations, such as ectopic thyroid tissue, accessory lobes, or lobar agenesis, were detected in the sample. All fetuses included in the study appeared morphologically normal externally, allowing for a uniform evaluation of thyroid development. The data were systematically recorded, tabulated, and subjected to statistical analysis for interpretation.

Table 1. Distribution of anomaly in human fetal thyroid gland.

S. No.	Gender	CRL (cm)	Wt (gms)	RTL (cm)	RTB (cm)	RTT (cm)	LTL (cm)	LTB (cm)	LTT (cm)	T Wt (gms)	Anomaly
1	M	13.5	180	0.8	0.3	0.2	0.5	0.3	0.3	0.043	Isth ab
2	F	21.3	1465	1.1	0.6	0.5	-	-	-	0.293	Isth ab

Abbreviations used: CRL - crown rump length, Wt - weight of fetus , RTL - right thyroid lobe length, RTB - right thyroid lobe breadth, RTT - right thyroid lobe thickness, LTL - left thyroid lobe length, LTB - left thyroid lobe breadth, LTT - left thyroid lobe thickness, T Wt - thyroid weight, Isth ab - Isthmus absent

DISCUSSION

Morphology

Gestational age is directly related to the growth of the thyroid gland. There may be many variations in size and shape of thyroid gland. These variations can be studied by many methods like, gross dissection, developmental anatomy and newer methods such as thyroid scans and scintigraphy. Many forms of thyroid gland can be found in human fetuses during early development. In rhesus monkey (Macacus rhesus), the thyroid glands are normal in position but there is no isthmus (Pastor et al, 2006) [14].

Marshall C F (1895), during his study on 60 cases, found complete isthmus agenesis only in 6 cases. Thus, the incidence of it came out to be 10% [15]. Allan FD in 1952 described about the isthmus agenesis in literature. According to him, the incidence of isthmus agenesis was 2-4 %.[16].

Duh et al (1994) and Burman et al (1975) stated that agenesis of isthmus can be associated with other types of dysorganogenesis such as absence of lobe or the presence of ectopic thyroid tissue hence in clinical practice when such a condition is diagnosed, it is necessary to perform a differential diagnosis against other pathologies such as thyroid nodule, primary carcinoma etc. [17,18]

Fabbro et al (1998) and Macchia et al (1999) described that several genes are responsible for control of thyroid development and morphogenesis and one of those genes is PAX8 [19,20]. Thyroid gland is well known for it's developmental anomalies ranging from common to rare (Moore and Persaud, 2003) [21].

Persistence of pyramidal lobe and thyroglossal duct cyst are common

anomalies whereas other rare anomalies are agenesis or hemiagenesis of thyroid gland, agenesis of isthmus alone or aberrant thyroid glands (Marshall,1895 and Testut,1978) [15,22].

Pastor et al. (2006) described isthmus agenesis as a congenital absence of the thyroid isthmus in Caucasian cadaver [14]. Macchia PE in 2000, described that TITF1, TITF2, PAX8 and TSHR genes are responsible for the normal development of the thyroid follicular cells. Mutation in these genes may lead to thyroid dysgenesis [20]. Won & Chung in 2002 had reported isthmus agenesis in 3% of the cases studied [23].

According to Karaby et al. (2003), the primary cause of isolated isthmus agenesis may be the failure of isthmus fusion in the midline [24]. Harjeet et al in 2004, during their study in north-west Indians found that the incidence of isthmus agenesis was 7.9% in gross specimens [25]. Gangbo et al (2004) described the chromosomal basis of isthmus agenesis. Chromosome 22 seems to be responsible for isthmus agenesis [26].

De Felice and Di Lauro in 2004 & Dumont and Vassart in 2005, described the genetic basis of thyroid developmental anomalies. They claimed that mutations in one of the three thyroid developmental genes—TITF1, PAX8, and FOXE1/TITF2—are the cause of the developmental agenesis [27,28].

Pastor Vazquez et al (2006) described that a fusion anomaly of the thyroglossal duct in midline leads to two independent lobes with no isthmus of the thyroid gland. They had reported the incidence of isthmus agenesis may vary from 5% to 10%. It is very hard to determine the actual incidence of thyroid isthmus agenesis [14]. Braun et al in 2007 mentioned the incidence of the isthmus agenesis to be 6.89% in cadavers [29].

Tonacchera et al (2007) tried to found out the etiology of agenesis of thyroid gland or isthmus agenesis. They inferred that most of the cases of isthmus agenesis are sporadic, familial or genetic predisposition [30]. During their study of 105 cadavers in 2008, Ranade et al found that the isthmus was absent in 35 (i.e. 33%) cadavers of which 8 were females [31].

Lania et al (2009) described that Tbx1-Fgf8 pathway regulates early thyroid development. Tbx1 regulates the size of the early thyroid primordium and expression of Fgf8 in the mesoderm and Fgf8 mediates critical Tbx1-dependent interactions between mesodermal cells and endodermal thyrocyte progenitors. Thus, they established that a Tbx1->Fgf8 pathway is a key size regulator of mammalian thyroid development [32].

During cadaveric dissection in 2010, Kumar et al. revealed isthmus agenesis and reported that the thyroid gland's right lobe was giving

Table 2. Incidence of Isthmus agenesis as recorded In previous years

S. No.	Authors	Incidence %	Year
1	Marshall [15]	8-10	1895
2	Allan [16]	2-4	1952
3	Anson [51]	6-8	1996
4	Won and Chung [23]	3	2002
5	Harjeet et al [25]	7.9	2004
6	Pastor Vazquez et al [14]	5-10	2006
7	Braun et al [29]	6.89	2007
8	Ranade et al [31]	33	2008
9	Dixit et al [5]	14.63	2009
10	Joshi S D et al [35]	16.66	2010
11	Tanriover et al [36]	2.22	2011
12	Devi sankar [39]	one case	2012
13	Krishnan et al [38]	one case	2012
14	Lokanadham et al [40]	one case	2012
15	Muktyaz et al [41]	12.5	2013
16	Kaur et al [42]	one case	2013
17	Kavyashree et al [43]	one case	2014
18	Lattupalli Hema [44]	79.5	2014
19	Shambhu Prasad et al [45]	one case	2014
20	VandanaTiwari et al [52]	one case	2015
21	Manish Gupta [53]	one case	2018
22	Tuore et al [49]	one case	2020
23	Saha et al [54]	one case	2023
24	Pushala et al [55]	one case	2024
25	Present study	**3.84**	2024

rise to the pyramidal lobe and levator glandulae thyroidae [33]. According to Sadler T. W. (2010), scintigraphy can be used to clinically diagnose isthmus agenesis in addition to other modalities such as magnetic resonance imaging (MRI), computerized tomography (CT), and ultrasound [34].

Joshi et al in 2010 studied 90 male cadavers and observed the incidence of isthmus agenesis as 16.66% [35]. Tanriover et al (2011), in their study observed that the isthmus was absent in 2 male cases out of a total of 90 cadavers (i.e. 2.22% incidence) [36].

In 2012 Kulkarni et al studied thyroid gland of 20 cadavers and stated that isthmus was absent in 10% of the cases [37]. Radhika Krishnan et al in 2012 during routine dissection noticed isthmus agenesis. Tracheal rings were exposed, and 2 separate lateral lobes of thyroid gland were present. Instead of the thyroid isthmus, the inferior thyroid vein is located on the tracheal rings; it formed a plexus and empties into the left brachiocephalic vein [38].

Devi Sankar et al (2012) described the genetic basis for isthmus agenesis and told that mutations in these genes were responsible for it, especially TITF1-2 genes [39]. Additionally, they documented a rare instance of thyroid gland isthmus agenesis and the origin of the pyramidal lobe with levator glandulae thyroidae from the thyroid gland's right lobe [39]. Lokanadham et al 2012 in their case study, observed isthmus agenesis in an aborted female fetus of 36 weeks of gestation. They also observed morphometric variations in each isolated lobe of thyroid gland [40].

Muktyaz et al (2013), in a study of 56 cases found that the isthmus was absent in 7 cases i.e. 12.5 % of which 2 (i.e.3.5%) were females [41]. When Kaur et al. performed a routine deep dissection of a female cadaver's neck in 2013, and found that the isthmus was missing, but both lateral lobes were in their normal positions. Both lobes had a normal nerve supply. There was no evidence of accessory thyroid tissue [42]. Kavyashree et al in 2014, revealed that a middle-aged male cadaver had isthmus agenesis, levator glandulae thyroidae, and a pyramidal lobe [43].

Lattupalli Hema (2014) stated that the isthmus was absent in 79.5% of cases in males and 72.7% of cases in females during her study on 50 cadavers [44]. Prasad et al (2014), during dissection found the two lobes of the thyroid were in their normal position but the isthmus was absent. Additionally, they saw levator glandulae thyroidae extending between the hyoid bone and the pyramidal lobe, as well as a pyramidal lobe extending upward from the left lobe [45].

Alfatani et al in 2014 studied 8 plastinated and 9 formalin fixed human thyroid gland and mentioned that the incidence of isthmus agenesis was 5.88% i.e. 1 specimen [46]. Yadav et al in 2014 performed their study on 26 cadavers and mentioned that the incidence of isthmus agenesis was 7.69% i.e. 2 cases out of 26 cases [47].

Archana Belavadi Jagadish et al in 2016 performed study on 30 apparently normal human cadavers and found that the incidence agenesis of isthmus of thyroid gland was 10% [48]. In 2020, Tuore T et al. noted that the thyroid isthmus was completely absent and that the superior and inferior thyroid arteries did not anastomose [49].

In their case report from 2024, Hamiedah et al. describe a very uncommon instance of thyroid isthmus agenesis linked to papillary thyroid carcinoma in a middle-aged woman. Even though the thyroid isthmus's absence alone is a benign congenital condition, it brings some special difficulties into the surgical management of thyroid malignancies. This case demonstrates the necessity for careful preoperative imaging to identify anatomic variations that can impact surgical strategy and performance [50].

From above discussion, as shown in Table 2, the incidence of isthmus agenesis varies greatly. In our study, we found the incidence of isthmus agenesis is 3.84 % in total. It is 1.92% both in males and females which is comparable with many authors. It is typically challenging to diagnose isthmus agenesis unless the patient is referred for another thyroid condition. When evaluating a missing thyroid isthmus on imaging, differential diagnoses should include solitary thyroid nodules, thyroiditis, malignancies, metastatic involvement, and infiltrative diseases such as amyloidosis. (Belavadi) [48].

CONCLUSION

Thyroid isthmus agenesis is uncommon in humans and has a 5–10% incidence rate. Rare and largely asymptomatic, agenesis of the isthmus is discovered by chance during imaging for another ailment. A differential diagnosis against other thyroid pathologies, such as metastases or autonomous thyroid nodules, is always required. The surgeon must search for ectopic thyroid nodules surrounding the normally located thyroid gland if they encounter isthmus agenesis either before or during thyroidectomy. An isolated isthmus agenesis may be primarily caused by failure of the isthmus fusion in the midline. Agenesis of the thyroid isthmus may be detected using imaging techniques such as ultrasound, CT, or MRI.

In the present study, we found isthmus agenesis which is a rare variation in thyroid gland. In our study the incidence of isthmus agenesis was found to be 3.84% total. It is 1.92% both in male and female fetuses which is comparable with many authors with a range of a case-16.66%.

REFERENCES

1. De Felice M, Di Lauro R. Thyroid development and its disorders: genetics and molecular mechanisms. Endocr Rev. 2004;25(5):722-746.
2. Macchia PE, Lapi P, Krude H, et al. PAX8 mutations associated with congenital hypothyroidism caused by thyroid dysgenesis. Nat Genet. 1998;19(1):83-86.
3. Dumont JE, Vassart G. Thyroid dysgenesis: genetic causes. Trends Endocrinol Metab. 2005;16(6):235-242.
4. Allan FD. Agenesis of the isthmus of the thyroid gland. Anat Rec. 1952;113:93–95.

5. Dixit D, Shilpa MB, Harsh MP, Ravishankar MV. Agenesis of isthmus of thyroid gland in adult human cadavers: a case series. Cases J. 2009;2:6640.
6. Ranade AV, Rai R, Pai MM, Nayak SR, Prakash, Krisnamurthy A, Narayana K. Anatomical variations of the thyroid gland: possible surgical implications. Singapore Med J. 2008;49(10):831–834.
7. Harjeet A, Sahni D, Jit I, Aggarwal AK. Shape, measurements and weight of the thyroid gland in northwest Indians. Surg Radiol Anat. 2004;26(2):91–95.
8. Pastor Vázquez J, Gil Verona JA, García-Consuegra L. Agenesis of the thyroid isthmus. Eur J Anat. 2006;10(2):83–86.
9. Sadler TW. Langman's Medical Embryology. 11th ed. Philadelphia: Lippincott Williams & Wilkins; 2010.
10. Karabay N, Comert A, Ozgur Z, et al. Morphometric details of the thyroid gland: a cadaveric study. Anat Sci Int. 2003;78(3):166–169.
11. Tonacchera M, De Marco G, Agretti P, et al. Identification and functional studies of two new PAX8 mutations associated with congenital hypothyroidism. J Clin Endocrinol Metab. 2007;92(2):428–433.
12. Kumar N, Aggarwal AK, Kumar Y, et al. Agenesis of the thyroid isthmus: a cadaveric study. Anat Sci Int. 2010;85(2):75–78.
13. Ajmani. Textbook of Embalming Principles and Legal Aspects. 1996:131–135.
14. Pastor VJ, Gil VJ, De Paz Fernández FJ, Barbosa Cachorro M. Agenesis of the thyroid isthmus. Eur J Anat. 2006;10(2):83–84.
15. Marshall CF. Variations in the form of the thyroid in man. J Anat Physiol. 1895;29:234–239.
16. Allan FD. An accessory or superficial inferior thyroid artery in a full term infant. Anat Rec. 1952;112:53.
17. Duh QY, Ciulla TA, Clark OH. Primary parathyroid hyperplasia associated with thyroid hemiagenesis and isthmus agenesis. Surgery. 1994;115:257–263.
18. Burman KD, Adler RA, Wartofsky L. Hemiagenesis of the thyroid gland. Am J Med. 1975;58:143–146.
19. Fabbro D, Pelizari L, Teli G, Damante G. Pax-8 protein levels regulate thyroglobulin gene expressions. J Mol Endocrinol. 1998;12:1100–1105.
20. Macchia PE. Recent advances in understanding the molecular basis of primary congenital hypothyroidism. Mol Med Today. 2000;6(1):36–42.
21. Moore KL, Persaud TVN. The Developing Human: Clinically Oriented Embryology. 7th ed. Philadelphia: Saunders; 2003. p.215–217.
22. Testut L, Latarjet A. Anatomia Humana. Tomo IV. Barcelona: Salvat; 1978. p.402–404.
23. Won HS, Chung IH. Morphological variations of the thyroid gland in Korean adults. Korean J Phys Anthropol. 2002;15:119–125.

24. Karaby N, Comlekci A, Canda MS, Bayraktar F, Degirmenci B. Thyroid hemiagenesis with multinodular goiter: A case report and review. Endocr J. 2003;50(4):409–413.
25. Harjeet A, Sahni D, Jit I, Aggarwal AK. Shape, measurements and weight of the thyroid gland in northwest Indians. Surg Radiol Anat. 2004;26:91–95.
26. Gangbo F, Lacombe D, Alberti EM, Taine L, Saura R, Carles DN. Trisomy 22 with thyroid isthmus agenesis and absent gallbladder. Genet Couns. 2004;15(3):311–315.
27. De Felice M, Di Lauro R. Thyroid development and its disorders: genetics and molecular mechanisms. Endocr Rev. 2004;25:722–746.
28. Dumont JE, Vassart G. Thyroid dysgenesis: multigenic or epigenetic or both? Endocrinology. 2005;146(12):5035–5037.
29. Braun EM, Windisch G, Wolf G, Hausleitner L, Anderhuber F. The pyramidal lobe: clinical anatomy and its importance in thyroid surgery. Surg Radiol Anat. 2007;29(1):21–27.
30. Tonacchera M, Banco ME, Montanelli L, Di Cosmo C, Agretti P, De Marco G. Genetic analysis of the PAX8 gene in children with congenital hypothyroidism and dysgenetic or eutopic thyroid glands: identification of a novel sequence variant. Clin Endocrinol (Oxf). 2007;67:34–40.
31. Ranade AV, Rai R, Pai MM, Nayak SR, Prakash, Krisnamurthy A, Narayana S. Anatomical variations of the thyroid gland: possible surgical implications. Singapore Med J. 2008;49(10):831–834.
32. Lania G, Zhang Z, Huynh T, Caprio C, Moon AM, Vitelli F, Baldini A. Early thyroid development requires a Tbx1-Fgf8 pathway. Dev Biol. 2009;328(1):109–117.
33. Kumar GP, Satyanarayana N, Vishwakarma N, Guha R, Dutta AK, Sunitha P. Agenesis of isthmus of thyroid gland, its embryological basis and clinical significance – a case report. Nepal Med Coll J. 2010;12(4):272–274.
34. Sadler TW. Langman's Medical Embryology. 11th ed. Philadelphia: Lippincott Williams & Wilkins; 2010. p.278–279.
35. Joshi SD, Joshi SS, Daimi SR, Athavale SA. The thyroid gland and its variations: a cadaveric study. Folia Morphol (Warsz). 2010;69(1):47–50.
36. Tanriover O, Comunoglu N, Eren B, Comunoglu C, Turkmen N, Bilgen S, et al. Morphometric features of the thyroid gland: a cadaveric study of Turkish people. Folia Morphol (Warsz). 2011;70(2):103–108.
37. Kulkarni V, Sreepadma S, Deshpande SK. Morphological variations of thyroid gland. Medica Innovatica. 2012;1(2):35–38.

38. Radhika Krishnan J, Priya G, Sundarapandian S. Agenesis of isthmus of thyroid gland – a cadaveric study. Int J Anat Sci. 2012;3(1):12–13.
39. Devi Sankar K, Sharmila Bhanu P, Bapuji P. Agenesis of isthmus of thyroid gland with embryological and clinical basis. NMJ. 2012;1(1):32–34.
40. Lokanadham S, Khaleel N, Sateesh Naik K, Subhadra Devi V. Multiple morphological variations of fetal thyroid glands in South Indian population. J Pharm Biomed Sci. 2012;15.
41. Muktyaz H, Birendra Y, Dhiraj S, Arun SK. Anatomical variations of thyroid gland and its clinical significance in north Indian population. GJBAHS. 2013;2(2):12–16.
42. Kaur HS, Kumar U, Bajwa SJS, Kalyan GS. Absent thyroid isthmus: embryological and clinical implications of a rare variation of thyroid gland revisited. Thyroid Res Pract. 2013;10(2):80–82.
43. Kavyashree AN, Asha KR, Bindurani MK, Lakshmi Prabha S. Agenesis of isthmus of thyroid gland with presence of pyramidal lobe and levator glandulae thyroideae. J Int Med Dent. 2014;1(2):93–96.
44. Lattupalli H. Multiple variations in the morphology of thyroid gland. Int J Recent Trends Sci Technol. 2014;11(2):143–147.
45. Prasad S, Singh R, Kumar N, Kumar S. Absence of isthmus of thyroid gland – a case report. IOSR J Dent Med Sci. 2014;13(7):32–34.
46. Alfatani EA, Zaki AI, El-Haggagy AA, Aal IHA. Anatomical variations of thyroid gland. Life Sci J. 2014;11(9):922–926.
47. Yadav A, Yadav M, Dixit A. A morphological study of levator glandulae thyroidae and pyramidal lobe in normal adult human thyroid gland. Int J Res Health Sci. 2014;2(4):1030–1033.
48. Jagadish AB, Prabhakar P, Subhash RLP. A cadaveric study of agenesis of isthmus of thyroid gland with embryological, genetic bases and clinical significance. Int J Anat Res. 2016;4(2):2386–2391.
49. Tuore T, Ba B, Kante A, Traore F, Kone M, Simpara G, et al. Agenesis of thyroid isthmus associated with a rare variation of origin of superior laryngeal and cricothyroid arteries: case report and review of the literature. Int J Anat Var. 2020;13(3):12–14.
50. Hamiedah MM, Al-Bdour B, Alshoubaki WI, Al-Nawaiseh HR, Aljaafreh HM. Thyroid isthmus agenesis coinciding with papillary thyroid carcinoma: a case report. Int J Adv Med. 2024;11(6):603–606.
51. Anson BJ. Morris' Human Anatomy. 12th ed. New York: McGraw-Hill; 1996. p.168–169.
52. Tiwari V, Rani A, Diwan RK, Verma RK, Pankaj AK. Agenesis of isthmus of thyroid gland: embryological basis – a case report. J Anat Sci. 2015;23(2):31–34.

53. Gupta M. Thyroid isthmus agenesis: a rare congenital anomaly. IP J Otorhinolaryngol Allied Sci. 2018;1(1):1–2.
54. Saha A, Saha S, Neha K. Agenesis of isthmus of thyroid gland – a case report. J Pharm Negative Results. 2023;14(2):622.
55. Pusala B, Rajasundaram A, Manoj KT, Johnson WM, Waghray N. A rare case of agenesis of isthmus with the presence of levator glandulae thyroideae in anterior lobulated thyroid gland. Oncol Radiother. 2024;18(6):1–4.

https://doi.org/10.46351/jas.v32i2pp112-125

JAS Journal of Anatomical Sciences (U.P. Chapter of Anatomical Society of India)

Original Article

Assessment of anatomical variations in retina, retinal vessels, retinal nerve fiber layer and macula in emmetropes and myopes using fundus camera and optical coherence tomography

Yagika Pareek[1], Anshu Gupta[1], Vibhu Deep[1], Kamal Bhardwaj[1], Pradeep Singh[1], Dinesh Pareek[2]

1. Department of Anatomy, Sarojini Naidu Medical College, Agra, India
2. Ophthalmologist & Director Blindness Control, MOHFW, Govt. of India

ABSTRACT

Introduction: Myopia is a prevalent refractive error characterized by axial elongation of the eyeball, frequently resulting in structural alterations within the retina and its microvasculature. Understanding these anatomical variations is crucial for differentiating physiological myopic changes from early pathological conditions such as glaucoma.

Materials and Methods: This cross-sectional observational study was conducted over one year on 200 subjects—100 diagnosed myopes and 100 age- and gender-matched emmetropic controls—at Sarojini Naidu Medical College, Agra. Following institutional ethical clearance and informed consent, all participants underwent detailed fundoscopic examination and optical coherence tomography (OCT). Parameters assessed included foveal, macular, perifoveal, and parafoveal thicknesses, retinal nerve fiber layer (RNFL) profiles, and retinal microvascular density.

Results: Myopic subjects demonstrated significantly reduced foveal, central foveal, and macular thickness compared to emmetropic controls ($p<0.05$). Greater degrees of myopia were associated with further thinning, particularly in the superior and inferior perifoveal regions. No significant variation was noted in parafoveal thickness. Retinal microvascular density and circularity index were markedly lower in myopes. Fundoscopic findings such as lattice degeneration, retinal tears, and posterior staphyloma were more frequently observed in the myopic group.

Conclusions: The study highlights distinct anatomical changes in myopic eyes, notably thinning in central and perifoveal retinal regions and reduced vascular density. These alterations must be considered during ocular evaluation to avoid misdiagnosis, particularly in distinguishing myopic changes from glaucomatous damage.

Keywords: Myopia, Emmetropia, Optical Coherence Tomography, RNFL, Retinal Thickness, Retinal Microvasculature

Address for Correspondence:
Dr. Anshu Gupta, Associate Professor & Head, Department of Anatomy, Sarojini Naidu Medical College, Agra, India
Email: ganshu19@gmail.com Mob.: 9359904089

Date of Receiving: 19 Nov 2024
Date of Acceptance: 27 Dec 2024

INTRODUCTION

Retina is a unique part of central nervous system & special senses. The ten layers of the retina from the innermost to the outermost, are named as follows: the inner limiting membrane, nerve fibre layer (NFL), ganglion cell layer (GCL), inner plexiform layer (IPL), inner nuclear layer (INL), outer plexiform layer (OPL), outer nuclear layer (ONL), external limiting membrane, photoreceptors layer (PL), and the retinal pigment epithelium (RPE).

Myopia, often known as near-sightedness, is a refractive defect. Light rays that originate at infinity and approach the eye parallel along the optic axis come to a focus on the front of the retina. This is typically produced by a comparatively lengthened eyeball from cornea to posterior pole, though it can also be brought on by a cornea that is excessively curved or by a lens that has more optical power. Both adults and children with myopia experience vision impairment, which can typically be treated with optical aids like contact lenses and glasses [1].

Myopia has been regarded as one of the most common ocular conditions due to its notable increase in incidence, especially in younger people in India and other Southeast and East Asian countries [2-7]. High myopia is thought to be one of the leading causes of permanent blindness and impaired vision globally since it is the main contributory factor in the onset of myopic maculopathy including excessive-myopia-associated glaucomatous as well as glaucoma-like optic neuropathy [8-10].

The myopization process and the underlying mechanisms that cause myopia have remained obscure up until now, despite its significance. It is possible to think of myopia as the outcome of an emmetropization failure stemming from an attempt to remove a relative hyperopic blurring in the periphery of an elliptical eye [11,12]. Knowing which tissue or ocular coat largely causes the eye to lengthen is a key question in comprehending the processes of emmetropization and myopization. The "retina, retinal pigment epithelium (RPE), Bruch membrane (BM), choroid, and/or sclera" are theoretical options [1].

Primary open angle glaucoma is also more likely in people with myopia who have anatomical characteristics involving alterations in the optic nerve, including a wide optic disc as well as optic tilt. The gold standard in diagnosing glaucoma is visual field measurement; however, structural abnormalities like flattening of the RNFL, that is primarily composed of ganglion cells and axons covered by astrocytes and processes of muller cells, occur before functional impairments. In as many as 60% of eyes, structural alteration is seen six years before any discernible visual field problems. Furthermore, the pathogenic mechanism of

myopia involves the RNFL. As a result, it can be utilized as a technique to diagnose early glaucoma, differentiate glaucoma from myopia, and comprehend the development of myopia [13].

OCT, or optical coherence tomography, enables non-invasive, potentially contact-free, high-resolution imaging of the RNFL. Since its initial introduction in 1991, this technology has undergone multiple generations of advancement [13].

Since anatomical discoveries could clarify the myopization process, we compared anatomical variations in retina and its microvasculature, foveal, perifoveal and parafoveal thickness in emmetropes and myopes using optical coherence tomography and ophthalmoscopy.

MATERIAL AND METHODS

This was a cross-sectional study conducted on 100 myopes and 100 emmetropes in Department of Anatomy, Sarojini Naidu medical college, Agra in collaboration with Department of Ophthalmology, in the study duration of 1 year between 2023-2024. After approval from IEC (institutional ethics committee) and taking informed consent from patients with myopia and healthy control as per ICH-GCP guidelines, the study was started.

Inclusion Criteria:

Case (Myopes/Group A): Myopia is defined as “a refractive error in which rays of light entering the eye parallel to the optic axis are brought to a focus in front of the retina with ocular accommodation at rest”. 50 patients with < - 6D acuity (Group A1) and 50 patients with > -6D (Group A2) were included in the study. Patients with age group of 20-40 years. Control (Emmetropes/Group B): Age and gender matched healthy controls.

Exclusion Criteria:

- Patients having history of glaucoma in family
- Patient with history of glaucomatous optic neuropathy
- Patients with history of eye or head trauma
- Patients with history of intraocular surgeries
- Patients with neurological diseases
- Patients with metabolic disorders (diabetic with diabetic retinopathy)
- Keratopathies/ keratoconus
- Patients on drug affecting the optic disc parameters

The anterior segment had been examined, initial VA was recorded, while the "best corrected visual acuity (BCVA) was documented. IOP determined by use of Schiotz tonometry. For dilatation, 2% homatropine is used in paediatric patients whereas 10 percent phenylephrine in adult patients. Using a direct as well as indirect ophthalmoscope, three mirrors, and a 90-degree lens, the fundus was inspected.

OCT was used to perform "dilated macular imaging" on the chosen study participants. Macular thickness was measured using and is characterized as the gap between "the inner boundary of RPE" to the ILM for each of the nine zones as determined by the previous research. 13 Four quadrants were created by dividing both "the inner and outer rings" into segments having radius of 1.5 millimetres and 3 millimetres, respectively. The mean thickness of the middle 1000 µm dimension of the previous research arrangement was referred to as foveal thickness.

The average thickness at the intersection of the six radial images was used to determine the "central foveal thickness". In each of the nine zones, digital measurements were made and recorded. Using the "International Nomenclature for OCT Panel and the structures' relative reflectivity", the anatomical features of the macula on OCT scans were identified. 14 The values produced by the program were contrasted with measures of "central foveal thickness" that had been measured manually. The evaluation included "the superior, inferior, nasal, and temporal quadrants" of the outer as well as inner rings as well as "the macular thickness of the central foveal area".

Statistical Analysis: The parameters measured from myopes and emmetropes were presented in tabular form using Microsoft Excel 2009 database standard and transferred to Minitab for further statistical analysis. OCT were expressed as mean ± SD and compared using unpaired t-test with $p<0.05$ as marker of statistical significance.

RESULTS

We have evaluated and compared retinal parameters and RNFL between myopes and emmetropes (Table 1, Table 3) and between myopes (<6D) and myopes (>6D) (Table 2, Table 4). The mean age of the patients enrolled for the study was 29.87 ± 4.68 years (range 20–40 years). There were 61% males in myopes as compared to 57% in emmetropes. (Figures 1-5)

Foveal thickness, and central foveal thickness was significantly lower in patients with high myopia as compared to patients with low myopia ($p<0.0001$). Perifoveal thickness in superior, inferior, and nasal was significantly lower in myopes as compared to emmetropes with respect to all quadrants ($P<0.05$).

There was no significant difference between myopes and emmetropes with respect to parafoveal thickness in any quadrant ($p>0.05$).

Micro vessels were significantly less dense in highly myopic eyes ($p<0.001$). The foveal avascular zone area was 0.35 ± 0.12 in myopes as compared to 0.46 ± 0.17 in emmetropes ($p<0.05$). Circularity index was 0.42 ± 0.09 in myopes as compared to 0.51 ± 0.16 in emmetropes ($p<0.05$).

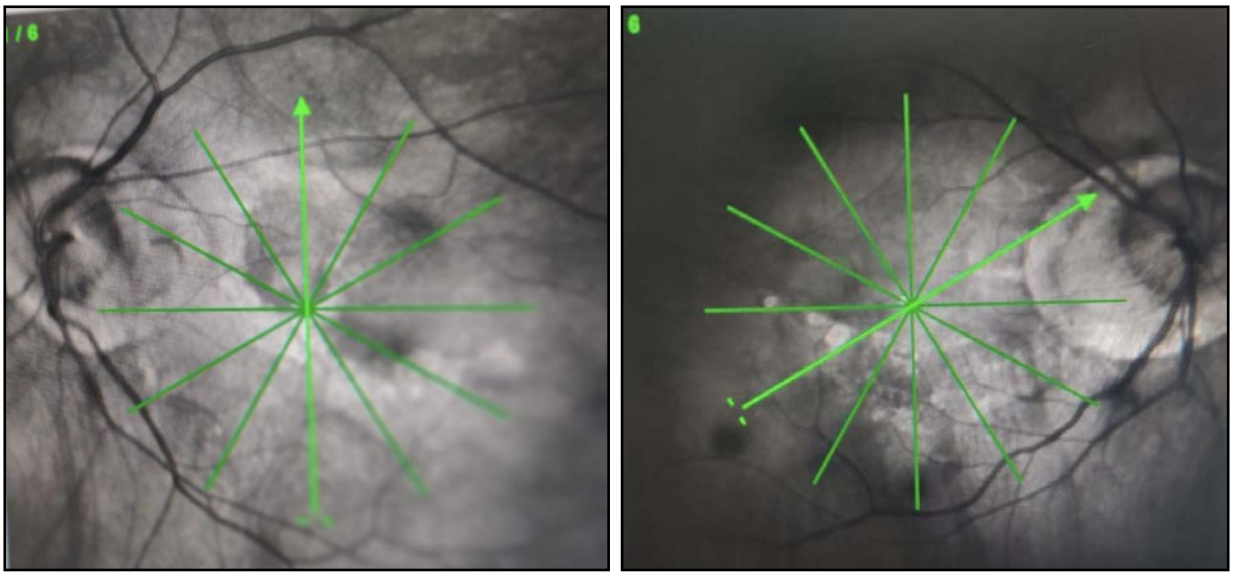

(a) (b)

Fig. 1. (a) Radial scan pattern centered on the macula in OCT imaging; (b) OCT radial scan centered on the optic nerve head

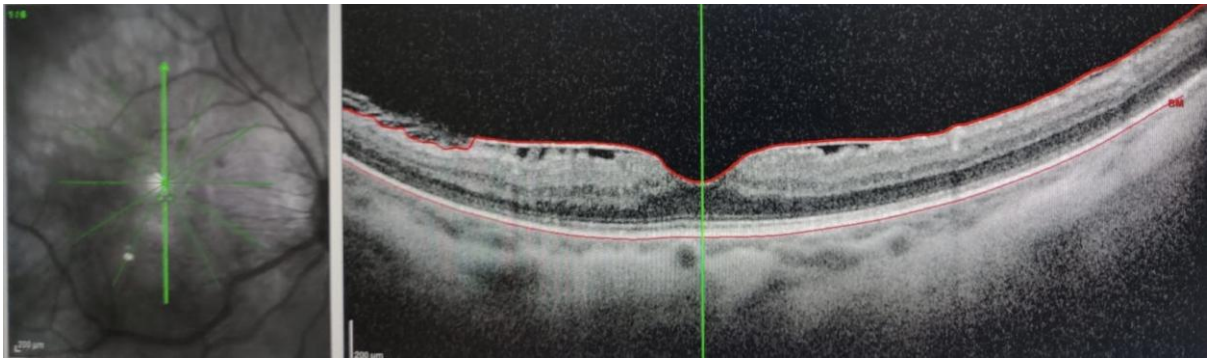

Fig. 2. Macular thickness mapping using OCT with cross-sectional B-scan. Composite image showing (left) the en face fundus view with radial scan lines centered on the macula and (right) the corresponding high-resolution B-scan OCT image.

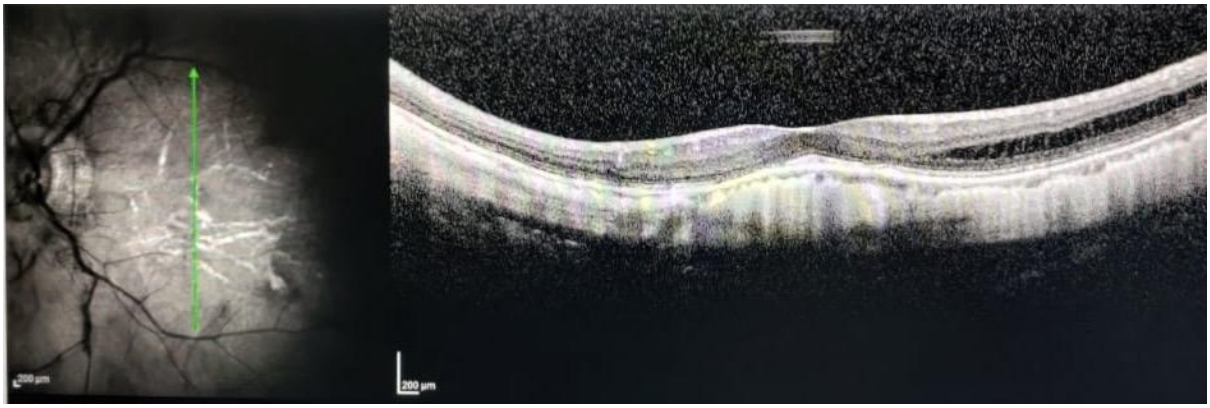

Fig. 3. OCT vertical B-scan of the macula showing retinal layer architecture. The left panel displays a fundus image with a vertical scan line passing through the foveal center, while the right panel shows the corresponding optical coherence tomography (OCT) B-scan.

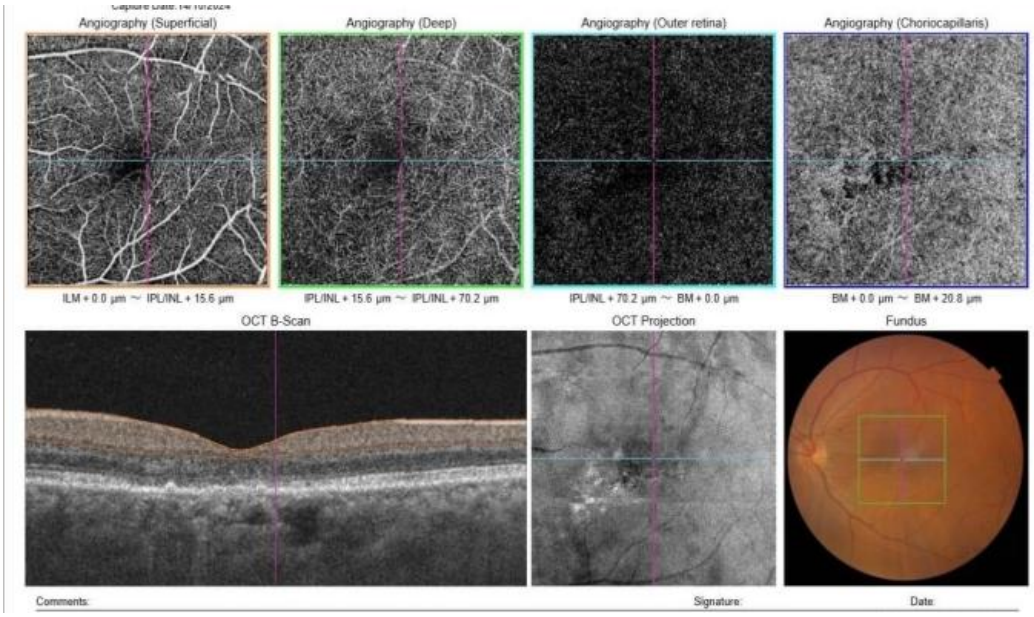

Fig. 4. Multilayer OCTA analysis showing retinal and choroidal vascular architecture. Top row - angiographic views of the superficial, deep, outer retina, and choriocapillaris layers; Bottom row - corresponding OCT B-scan, OCT projection map, and color fundus image centered on the macula.

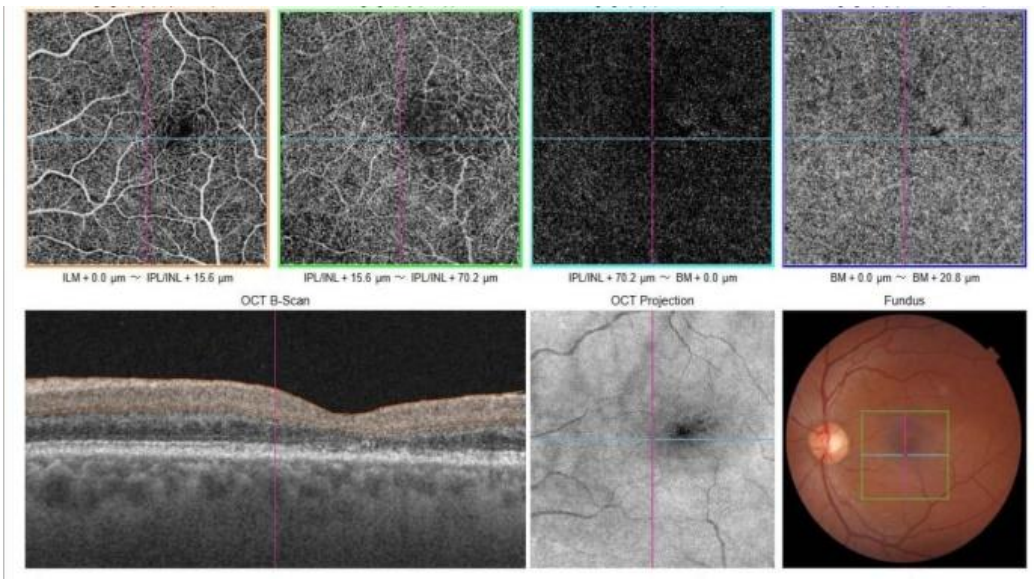

Fig. 5. Layer-wise OCTA and structural correlation in a healthy emmetropic eye. Top row - Multiplanar OCT angiography (OCTA) montage illustrating microvascular patterns across different retinal and choroidal layers: superficial plexus, deep plexus, outer retina, and choriocapillaris; Bottom row - corresponding structural OCT B-scan, en face OCT projection, and color fundus image centered on the fovea. Crosshairs denote the scan axis across all panels.

Table 1. Comparison of Foveal and Macular Thickness between Myopes (Group A) and Emmetropes (Group B)

Parameters	Parameters in (Mean ± SD)		P-Value (Unpaired t test)
	Group A (n=100)	Group B (n = 100)	
Foveal Thickness	231.78 ± 15.36	239.42 ± 18.27	0.002
Central Foveal Thickness	163.66 ± 9.87	171.64 ± 11.49	<0.0001
Macular Thickness	278.72 ± 17.43	284..98 ± 19.62	0.02

Table 2. Comparison of Foveal and Macular Thickness between Group A1 (<6D) and Group A2 (>6D) in Myopes

Parameters	Parameters in in µm (Mean ± SD)		P-Value (Unpaired t test)
	Group A1 (n=50)	Group A2 (n = 50)	
Foveal Thickness	234.96 ± 15.47	227.64 ± 14.21	0.02
Central Foveal Thickness	165.54 ± 8.79	160.18 ± 10.53	0.006
Macular Thickness	281.50 ± 16.23	275.02 ± 18.49	0.06

Table 3. Comparison of Perifoveal Thickness between Myopes (Group A) and Emmetropes (Group B)

Quadrant	Perifoveal Thickness in µm (Mean ± SD)		P-Value (Unpaired t test)
	Group A (n=100)	Group B (n = 100)	
Inferior	261.45 ± 15.47	267.25 ± 17.63	0.01
Superior	272.59 ± 16.94	278.50 ± 19.87	0.02
Nasal	288.15 ± 18.14	295.53 ± 19.61	0.0006
Temporal	253.39 ± 17.20	256.62 ± 18.67	0.20

Table 4. Comparison of Parafoveal Thickness between Myopes (Group A) and Emmetropes (Group B)

Quadrant	Parafoveal Thickness in µm (Mean ± SD)		P-Value (Unpaired t test)
	Group A (n=100)	Group B (n = 100)	
Inferior	304.25 ± 20.47	309.01 ± 22.58	0.12
Superior	303.93 ± 19.59	309.28 ± 21.86	0.07
Nasal	307.64 ± 22.76	313.26 ± 24.25	0.09
Temporal	296.51 ± 21.67	298.25 ± 22.69	0.58

Table 5. Total Vessel Density (Dbox) in the Different Retinal Layers of between Myopes (Group A) and Emmetropes (Group B)

Vessel Patterns	Total Vessel Density (D_{box}) (Mean ± SD)		P-Value (Unpaired t test)
	Group A (n=100)	Group B (n = 100)	
Superficial Micro vessels	1.73 ± 0.02	1.76 ± 0.01	<0.0001
Superficial Large Vessels	1.04 ± 0.03	1.07 ± 0.02	<0.0001
Deep Micro vessels	1.75 ± 0.02	1.78 ± 0.01	<0.0001
Deep Large Vessels	1.04 ± 0.02	1.06 ± 0.02	<0.0001
Whole Retina Micro Vessels	1.76 ± 0.02	1.79 ± 0.01	<0.0001
Whole Retina Large Vessels	1.05 ± 0.02	1.06 ± 0.01	<0.0001

Table 6. Comparison of Fundus Changes observed under Ophthalmoscopic Changes between Myopes (Group A) and Emmetropes (Group B).

Fundus Changes	Number of Patients (%)		P-Value (Unpaired t test)
	Group A A1+A2 (n=100)	Group B (n = 100)	
Lattice Degeneration	5	31	<0.0001
Chorioretinal degeneration	2	4	0.68
White with pressure/ white without pressure	6	22	0.001
Retinal tear	1	13	0.001
Retinal detachment	5	13	0.08
Posterior staphyloma	1	10	0.01

Lattice Degeneration, white with pressure/ white without pressure, retinal tear, retinal detachment, and posterior staphyloma were significantly greater in myopes as compared to emmetropes ($p<0.05$).

DISCUSSION

The average thickness of the retinal nerve fiber layer (RNFL) became thinner as the degree of myopia increased in our study. It was shown that there was a statistically significant drop between emmetropes and myopes. These results are in line with those of earlier research by Wang et al., Ozdek et al., as well as Savini et al., who also found that the mean peripapillary RNFL thickness decreased significantly ($P < 0.05$) as myopia increased [15-17].

The study revealed that the RNFL thickness in the inferior quadrant was the thickest, with the superior, nasal, as well as temporal quadrants following suit. The results of Kamath et al. as well as Said-Ahmed et al. are comparable [18,19]. Both upper and lower quadrants showed a significant reduction in quadrant-based RNFL thickness as there was more myopia. Our findings are in line with those of Wang et al. and Ozdek et al., who observed an insignificant change in the nasal and temporal quadrants but a substantial reduction in RNFL thickness only for the superior or inferior quadrants [15,16]. Nonetheless, Kamath and colleagues documented a reduction in RNFL thickness throughout all quadrants, accompanied by a negligible decline in the temporal quadrant [18].

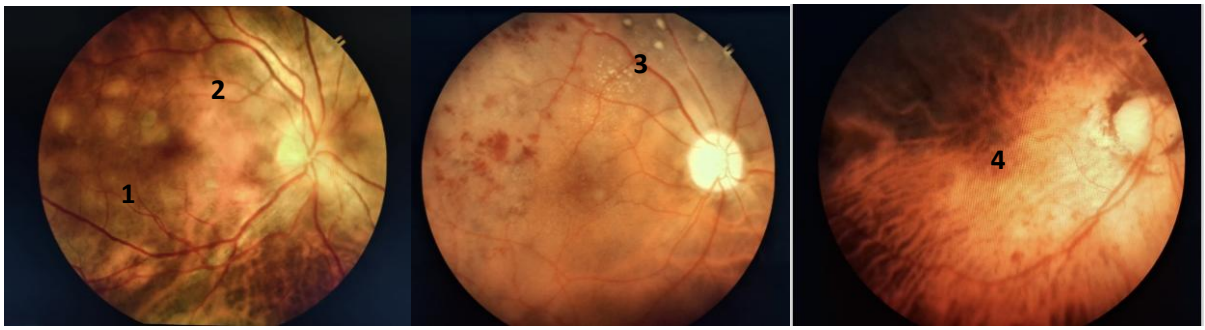

Fig. 6. 1. Peripheral chorioretinal degeneration; 2. Peripheral retinal thinning; 3. Lattice degeneration; 4. Tessellated fundus

With the exception of the 4, 8, and 10 o'clock locations, RNFL thickness decreases as myopia increases in all clock-hour positions [19]. In hyper myopia eyes (>6 D), Kamath et al. observed a substantial decrease in the thickness of the RNFL in all clock-hour locations with the exception of 4, 8, 9, and 10 o'clock [18]. The degree of myopia and the thickness of the RNFL in the inferior quadrant showed a somewhat positive connection. This result is consistent with research conducted by Mohammad as well as Rauscher et al [20,21].

Except the rim area, which showed a rise, all optic nerve head characteristics in our study showed a decline with increasing myopia. This finding is consistent with research by Tsutsumi et al. as well as Sujatha et al. that showed that as myopia increased, there was a drop in "cup area, cup volume, and cup-to-disc ratio" in addition to lower disc areas [22,23]. When compared to emmetropic eyes, eyes with extreme myopia (>6 D) have a much greater rim volume, according to studies by AttaAllah et al., Hsu et al., as well as Bhaila et al [24-26].

The optic nerve is inserted obliquely in high myopia eyes because the scleral canal takes an oblique path that is further toward the nasal part of the orbit [27,28]. As a result, the temporal part of the optic disc becomes posteriorly depressed and gets concealed in the scleral canal, while the nasal portion of the disc is elevated anteriorly. Therefore, disc tilt rises with increasing myopia, leading to incorrect perceptions of optic disc parameters. The dispersion of the nerve fibers throughout the temporal quadrant, which is the weakest according to our findings, may also be caused by disc tilt.

Retinal degeneration in severely myopic eyes can lead to decreased blood supply needs, which can result in a decrease in microvessel density. On the other hand, axial lengthening, which appears to inevitably stretch the retinal vascular, may have compromised the retinal vasculature and contributed to the retinal impairment. It's a chicken-and-egg situation as to which occurs first, and further longitudinal research is necessary. In very myopic eyes, retinal vessel diameter narrowing may potentially be a factor in

decreased density since capillary network loss is probably the outcome of decreased retinal blood circulation. There have been reports of decreased blood flow to the retina as well as retrobulbar blood vessels in highly myopic eyes [29-30].

In myopia patients, lattice degeneration was more frequently observed in the supero-temporal quadrant. This is most likely the result of this area's enhanced vascularity and severe straining. Retinal detachment as well as lattice are associated because vitreous adherence is frequently observed on the lattice's edge. "White without pressure" is important because it shows some "vitreoretinal adhesion" as well as thinning in this location. Ruptures of the retina were linked to degenerative alterations in the retina in about 10% of patients.

Retinal detachment was not present in patients with chorioretinal degeneration. The strong adherence of the choroid and retina is the cause of this. Retinal detachment was more common among people having moderate to profound myopia. "Breaks, lattice degeneration, as well as vitreous degeneration" were the causes of this. The retinal breaks were not localized in this case, as there was a marked decline in vision [31].

A bigger sample size, a single operator conducting the tests, and repeated OCT scanning (a mean of three measurements were taken) are possible advantages of our study. One limitation of the current study is that it focused solely on patients from northern India, making it unable to extrapolate the results to other groups.

CONCLUSION

In this cross-sectional study, foveal as well as perifoveal thickness were found to be lower in myopes as compared with emmetropes. There were significantly more cases of lattice degeneration, and retinal tear in myopes. Retinal vascularity was also less dense in myopes. In myopic individuals, RNFL thinning may be mistakenly identified as glaucomatous damage if the influence of Spherical Equivalence and Axial Length is not taken into consideration, and the existing nomograms are not adjusted for them. OCTA pictures can be used for fractal evaluation of the microvasculature, which could aid in identifying the pathological processes that underlie high myopia.

REFERENCES

1. Patel A, Patel D, Prajapati V, Patil MS, Singhal D. A study on the association between myopia and elevated intraocular pressure conducted at a tertiary care teaching hospital in Gujarat, India. Cureus. 2022 Aug 18;14(8):e28128. doi: 10.7759/cureus.28128. PMID: 36134039; PMCID: PMC9482132.
2. Congdon N, Wang Y, Song Y, et al. Visual disability, visual function, and myopia among rural Chinese

secondary school children: the Xichang Pediatric Refractive Error Study (X-PRES)–report 1. Invest Ophthalmol Vis Sci. 2008;49:2888–94.

3. Morgan IG, Ohno-Matsui K, Saw SM. Myopia. Lancet. 2012;379:1739–48.
4. Guo K, Yang DY, Wang Y, et al. Prevalence of myopia in school children in Ejina. The Gobi Desert Children Eye Study. Invest Ophthalmol Vis Sci. 2015;56:1769–74.
5. Wu JF, Bi HS, Wang SM, et al. Refractive error, visual acuity and causes of vision loss in children in Shandong, China. The Shandong Children Eye Study. PLoS One. 2013;8:e82763.
6. You QS, Wu LJ, Duan JL, et al. Prevalence of myopia in school children in greater Beijing: the Beijing Childhood Eye Study. Acta Ophthalmol. 2014;92:e398–406.
7. Dong L, Kang YK, Wei WB, et al. Prevalence and time trends of myopia in children and adolescents in China: a systematic review and meta-analysis. Retina. 2019; [accepted].
8. Ohno-Matsui K, Kawasaki R, Jonas JB, et al. International classification and grading system for myopic maculopathy. Am J Ophthalmol. 2015;159:877–83.
9. Xu L, Wang Y, Wang S, et al. High myopia and glaucoma susceptibility. The Beijing Eye Study. Ophthalmology. 2007;114:216–20.
10. Holden BA, Fricke TR, Wilson DA, et al. Global prevalence of myopia and high myopia and temporal trends from 2000 through 2050. Ophthalmology. 2016;123:1036–42.
11. Smith EL 3rd, Hung LF, Huang J, et al. Effects of optical defocus on refractive development in monkeys: evidence for local, regionally selective mechanisms. Invest Ophthalmol Vis Sci. 2010;51:3864–73.
12. Smith EL 3rd. Prentice Award Lecture 2010: a case for peripheral optical treatment strategies for myopia. Optom Vis Sci. 2011;88:1029–44.
13. Early Treatment Diabetic Retinopathy Study design and baseline patient characteristics. ETDRS report number 7. Ophthalmology. 1991;98(5 Suppl):741–56.
14. Staurenghi G, Sadda S, Chakravarthy U, Spaide RF; International Nomenclature for Optical Coherence Tomography (IN•OCT) Panel. Proposed lexicon for anatomic landmarks in normal posterior segment spectral-domain optical coherence tomography: the IN•OCT consensus. Ophthalmology. 2014;121:1572–8.
15. Wang G, Qiu KL, Lu XH, Sun LX, Liao XJ, Chen HL, et al. The effect of myopia on retinal nerve fibre layer measurement: a comparative study of spectral-domain optical coherence tomography and scanning laser polarimetry. Br J Ophthalmol.

2011;95:255–60.

16. Ozdek SC, Onol M, Gürelik G, Hasanreisoglu B. Scanning laser polarimetry in normal subjects and patients with myopia. Br J Ophthalmol. 2000;84:264–7.
17. Savini G, Barboni P, Parisi V, Carbonelli M. The influence of axial length on retinal nerve fibre layer thickness and optic-disc size measurements by spectral-domain OCT. Br J Ophthalmol. 2012;96:57–61.
18. Kamath AR, Lakshey D. Peripapillary retinal nerve fibre layer thickness profile in subjects with myopia measured using optical coherence tomography. J Clin Ophthalmol Res. 2014;2:131–6.
19. Said-Ahmed KEG, Inbrahem AMA, Salama AA. Association of retinal nerve fibre layer thickness and degree of myopia using spectral-domain optical coherence tomography. Menoufia Med J. 2017;30:966–70.
20. Salih PA. Evaluation of peripapillary retinal nerve fiber layer thickness in myopic eyes by spectral-domain optical coherence tomography. J Glaucoma. 2012;21:41–4.
21. Rauscher FM, Sekhon N, Feuer WJ, Budenz DL. Myopia affects retinal nerve fiber layer measurements as determined by optical coherence tomography. J Glaucoma. 2009;18:501–5.
22. Tsutsumi T, Tomidokoro A, Saito H, Hashizume A, Iwase A, Araie M. Confocal scanning laser ophthalmoscopy in high myopic eyes in a population-based setting. Invest Ophthalmol Vis Sci. 2009;50:5281–7.
23. Sujatha R, Maqbool A. Analysis of optic disc and peripapillary area using optical coherence tomography in young adult Indian myopic eyes at Ambedkar Medical College. J Evid Based Med Healthc. 2016;3:777–85.
24. AttaAllah HR, Omar IAN, Abdelhalim AS. Evaluation of optic nerve head parameters and retinal nerve fiber layer thickness in axial myopia using SD OCT. Ophthalmol Ther. 2017;6:335–41.
25. Hsu SY, Chang MS, Ko ML, Harnod T. Retinal nerve fibre layer thickness and optic nerve head size measured in high myopes by optical coherence tomography. Clin Exp Optom. 2013;96:373–8.
26. Bhaila S, Joshi SN, Thapa M, Shrestha GS. Effect of high myopia on optic nerve head by confocal scanning laser ophthalmoscopy in Nepalese eyes. Korean J Ophthalmol. 2019;33:181–8.
27. Yanoff M, Fine BS. Ocular Pathology. 3rd ed. Philadelphia: JB Lippincott; 1989. p. 84.
28. Chihara E, Sawada A. Atypical nerve fiber layer defects in high myopes with high-tension glaucoma. Arch Ophthalmol. 1990;108:228–32.
29. Li H, Mitchell P, Rochtchina E, et al. Retinal vessel caliber and myopic retinopathy: the Blue Mountains Eye Study. Ophthalmic Epidemiol.

2011;18:275–80.

30. Hollo G, Greve EL, van den Berg TJ, Vargha P. Evaluation of the peripapillary circulation in healthy and glaucoma eyes with scanning laser Doppler flowmetry. Int Ophthalmol. 1996;20:71–7.
31. Manickavelu BM, Kannan T. Correlation of fundus changes in relation to refractive error in patients with myopia—a clinical prospective study. J Evid Based Med Healthc. 2018;5(3):233–6.